JCI The Journal of Clinical Investigation

Molecular cross-talk between Y5-receptor and neuropeptide Y drives liver cancer

Peter Dietrich, … , Anja Bosserhoff, Claus Hellerbrand

J Clin Invest. 2020. https://doi.org/10.1172/JCI131919.

Research In-Press Preview Aging Hepatology

Graphical abstract

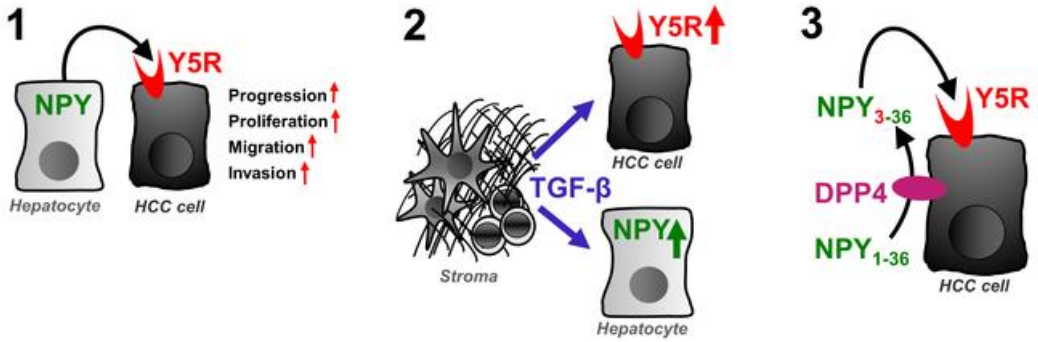

Molecular cross-talk between Y5-receptor and neuropeptide Y drives liver cancer

Peter Dietrich[1,2,#], Laura Wormser[1], Valerie Fritz[1], Tatjana Seitz[1], Monica De Maria[3], Alexandra Schambony[3], Andreas E. Kremer[2], Claudia Günther[2], Timo Itzel[4], Wolfgang E. Thasler[5], Andreas Teufel[4], Jonel Trebicka[6], Arndt Hartmann[7,8], Markus F. Neurath[2,8], Stephan von Hörsten[9], Anja K. Bosserhoff[1,8,*], Claus Hellerbrand[1,8,*,#]

[1]Institute of Biochemistry, Emil-Fischer-Zentrum, Friedrich-Alexander-University Erlangen-Nürnberg, Erlangen, Germany
[2]Department of Medicine 1, University Hospital Erlangen, Friedrich-Alexander-University Erlangen-Nürnberg, Erlangen, Germany
[3]Biology Department, Developmental Biology, Friedrich-Alexander University Erlangen-Nürnberg, Erlangen, Germany
[4]Department of Internal Medicine II, Medical Faculty Mannheim, Heidelberg University, Mannheim, Germany
[5]Hepacult GmbH, Am Klopferspitz 19, D-82152 Planegg/Martinsried, Germany
[6]Department of Medicine I, University Hospital Bonn, Bonn, Germany
[7]Institute of Pathology, Friedrich-Alexander-University Erlangen-Nürnberg, Germany
[8]Comprehensive Cancer Center (CCC) Erlangen-EMN, Erlangen, Germany
[9]Department of Experimental Therapy, Franz-Penzoldt-Center, Friedrich-Alexander-University Erlangen-Nürnberg, Erlangen, Germany

* Equal contribution

[#] Corresponding authors:

Claus Hellerbrand, MD
Institute of Biochemistry, Emil-Fischer Zentrum
Friedrich-Alexander-University Erlangen-Nürnberg
Fahrstraße 17
91054 Erlangen, Germany
Phone: +49 9131 85 24644
Email: claus.hellerbrand@fau.de

Peter Dietrich, MD, PhD
Department of Medicine 1
University Hospital Erlangen
Ulmenweg 18
91054 Erlangen, Germany
Phone: +49 9131 85 45221
Email: peter.dietrich@fau.de

Conflict of interest statement: All authors declare that no conflict of interest exists.

ABSTRACT

Hepatocellular carcinoma (HCC) is clearly age-related and represents one of the deadliest cancer types worldwide. Due to globally increasing risk factors including metabolic disorders, the incidence rates of HCC are still rising. However, the molecular hallmarks of HCC remain poorly understood. Neuropeptide Y (NPY) and NPY-receptors represent a highly conserved, stress-activated system which is involved in diverse cancer-related hallmarks including aging and metabolic alterations, but its impact on liver cancer had been unclear. Here, we observed increased NPY5-receptor (Y5R) expression in HCC which correlated with tumor growth and survival. Furthermore, we found that its ligand NPY was secreted by peri-tumorous hepatocytes. Hepatocyte-derived NPY promoted HCC progression by Y5R-activation. Transforming growth factor beta 1 (TGFβ1) was identified as a regulator of NPY in hepatocytes and induced Y5R in invasive cancer cells. Moreover, NPY-conversion by dipeptidylpeptidase 4 (DPP4) augmented Y5R-activation and function in liver cancer. The TGFβ-NPY-Y5R-axis and DPP4 represent attractive therapeutic targets for controlling liver cancer progression.

INTRODUCTION

Hepatocellular carcinoma (HCC) is the fourth most common cause of cancer related mortality worldwide and one of the cancers with still increasing incidence rates (1). Major risk factors are chronic infection with hepatitis B and C viruses and alcohol abuse (1). However, also non-alcoholic fatty liver disease (NAFLD) which is associated with obesity, insulin resistance, and type 2 diabetes, represents an increasingly recognized trigger for HCC development, especially in developed countries (1, 2). In this context, advanced age has been reported to predispose to HCC and indeed, HCC is mainly affecting those in the age of 65 years and older (3). Likewise, aging is recognized as significant and independent risk factor for cancer (4, 5). Hallmarks of cancer development and progression resemble hallmarks of aging, including cellular stress, autophagy, and deregulated nutrient sensing which is correlated with metabolic disorders such as obesity, insulin resistance and NAFLD (6, 7).

Human aging is tightly linked to activation of the stress-induced sympathoadrenergic system (8, 9). Moreover, sympathoadrenergic signaling has emerged as a strong promoter of several cancer types (10-13). Sympathoadrenergic effects are mediated by catecholamines and the highly conserved neuropeptide Y (NPY). NPY is one of the most widely expressed neurotransmitters in the central and peripheral nervous systems (14). NPY signals via binding and activation of the G-protein coupled receptors Y1R, Y2R, and Y5R (15). Herewith, NPY plays a crucial role in various biological processes including cortical excitability, stress response, food intake, circadian rhythms and cardiovascular function (16). Several milestone studies also suggested key roles of the NPY-system in the regulation of diverse common hallmarks of aging, metabolic disorders and cancer (17), including autophagy (18), nutrient sensing, caloric restriction, appetite regulation (19-21), mitochondrial dysfunction (22),

cell proliferation (23) and hematopoietic stem- and progenitor-cell properties like migration and intra-/extravasation (24).

With regards to the liver, systemic NPY levels have been described as potent modulators of chronic liver disease (25-28). NPY affects hepatic lipid and glucose metabolism in a way favoring the development of hepatic steatosis, and knockdown of NPY in the hypothalamus promotes hepatic insulin sensitivity in rats (29). Accordingly, transgenic overexpression of NPY in noradrenergic neurons increased hepatic levels of triglycerides and cholesterol in mice (30). Furthermore, NPY controls hepatic very low-density lipoprotein (VLDL)-triglyceride secretion via the sympathetic nervous system (31). Moreover, an in vitro study revealed that NPY promoted the proliferation of activated hepatic stellate cells which could impact hepatic fibrosis (28). Further studies demonstrated pronounced vasoactive effects of NPY in portal hypertension, which represents a life-threatening complication of advanced liver cirrhosis (25-27). However, the role of the NPY-system in liver cancer remained elusive and has now been addressed in this study.

RESULTS

Enhanced Y5-receptor expression in a spontaneous mouse model of liver cancer and in patients with hepatocellular carcinoma

Although spontaneous hepatocarcinogenesis in aged C3H/HeN mice was first described in the year 1960, the underlying mechanisms are still unknown (32-38). Since the NPY-system was linked to hallmarks of aging, C3H/HeN mice were chosen as a model system to explore age-related gene expression patterns of the NPY-system in hepatocarcinogenesis. Eighty percent of aged (>18 months) male C3H/HeN mice exhibited macroscopic liver tumors (**Figure 1A**). Histological analysis revealed diverse HCC-related growth patterns representing inter- and intra-tumorous heterogeneity as frequently observed in murine and human HCC (39-41) (**Figure 1B**). Analysis of surrounding non-tumorous liver tissue revealed that as compared with young mice, significantly higher Y5R mRNA expression was detected in aged mice, while Y1R, Y2R and NPY expression levels showed no age-dependent differences (**Figure 1C**). Age-dependent upregulation of hepatic Y5R (but not Y1R and Y2R) mRNA levels was also found in Gene Expression Omnibus (GEO) datasets derived from mouse and rat models (**Figure S1A**,**B**). On the protein level, immunohistochemical analysis confirmed higher Y5R expression in livers of aged as compared with young C3H/HeN mice (**Figure 1D**; **Figure S1C**).

Strikingly, in HCC tissues of aged C3H/HeN mice, Y5R mRNA and protein levels were even further upregulated as compared to corresponding non-tumorous liver tissues (**Figure 1E,F**; **Figure S1D**), while no cancer-related upregulation was found for NPY, Y1R and Y2R (**Figure 1E**).

Applying patient-derived samples, Y5R mRNA and protein expression levels were confirmed to be low in non-tumorous liver tissues but also increased with age (**Figure**

1G; **Figure S1E-G**; **Table S3**). Moreover, Y5R mRNA levels were further upregulated in human HCC tissues (**Figure 1H**). Immunohistological analysis of a tissue microarray (TMA) comprising paired samples of human HCC tissues and corresponding non-tumorous liver samples of the same patient (42-44) confirmed strong expression and marked upregulation of Y5R protein expression in HCC (**Figure 1I**; **Figure S1H**,**I**; **Table S1**).

Overexpression of both mRNA and protein levels of Y5R pointed to transcriptional upregulation in HCC. Screening of the "Catalogue of Somatic Mutations in Cancer" (COSMIC) database revealed age-associated hypomethylation of a CpG-island within the Y5R gene applying human "The Cancer Genome Atlas" (TCGA)-derived HCC samples (**Figure S1J**). Further analysis (applying the "MethHC" database (45) and the same TCGA cohort) revealed age-related hypomethylation of four additional CpG-sites within the Y5R promotor region, which was inversely correlated with Y5R expression (**Figure 1SK**,**L**). These findings link age-dependent differential methylation of Y5R with enhanced gene expression in HCC. Alterations in DNA-methylation have been described as a molecular link between aging and caner (46), were shown to occur in most cancer types and can induce genomic instability and liver cancer formation (47-49).

Together, the upregulation of Y5R expression in liver cancer prompted us to ask whether this NPY-receptor might have functional impact in HCC.

Y5R enhances tumorigenicity of HCC and correlates with tumor progression and poor survival

Y5R was also strongly overexpressed in human HCC cell lines as compared with primary human hepatocytes (**Figure 2A**,**B**). Its ligand NPY was abundantly detected in the serum which had been added to the cell culture medium for functional in vitro

analysis (**Figure S2A**). Si-RNA-Pool-mediated knockdown of Y5R (**Figure S2B**) induced strong reduction of Ki-67 expression and proliferation in HCC cells (**Figure 2C**,**D**; **Figure S2C**). Fitting to these in vitro findings, Y5R expression levels correlated with CyclinD1 and Ki67 expression in HCC tissues (**Figure 2E**; **Figure S2D**). Furthermore, Y5R-knockdown markedly reduced both number and size of colonies formed by HCC cells applying clonogenicity assays (**Figure 2F**; **Figure S2E**). Stem cell properties including enhanced clonogenicity are well-known to contribute to HCC development and progression (50).

Analysis of several different TCGA-datasets revealed enhanced Y5R expression in high-risk compared with low-risk (based on prognostic index) HCC patient groups. Furthermore, high Y5R expression was also associated with poor overall and recurrence free survival (**Figure 2G**; **Figure S2F**) as well as with advanced tumor stages (**Figure S2G**) in HCC patients. In line with this, immunohistochemical analysis of human HCC tissues derived from a further patient cohort (tissue micro array) confirmed that high Y5R expression was correlated with poor patient survival (**Figure 2H**; **Figure S2H**; **Table S2**) and advanced tumor stages (**Figure 2I**; **Table S2**).

In summary, these data indicated enhanced Y5R expression in HCC as promoter of tumor progression and suggested this NPY-receptor as a prognostic and potential therapeutic target.

Y5R-inhibition impairs tumorigenicity and growth of HCC

The emerging role of the Y5R-NPY-axis in obesity (51) has inspired the development of several small molecules for pharmacologic Y5R-inhibition. "CGP71683" (Y5R-Inh) (**Figure 3A**) inhibits Y5R with high affinity and selectivity towards other NPY-receptors (**Figure S3A**) (52). In vitro, this Y5R-inhibitor dose-dependently reduced proliferation and induced G0/G1-cell cycle arrest in human HCC cells (**Figure 3B,C**; **Figure**

S3B,C). Clonogenicity assays revealed marked reduction of colony numbers and sizes after treatment with this inhibitor (**Figure 3D**). These effects of pharmacologic Y5R-inhibition on proliferation and clonogenicity were confirmed using three further specific small molecule Y5R-inhibitors (53, 54) (**Figure S3A**; **Figure S3D-F**).

Also in murine HCC cells (including Hepa129 which originate from C3H mice (55)), Y5R was overexpressed as compared to murine hepatocytes (**Figure S3G**,**H**), and pharmacologic Y5R-inhibition showed strong anti-tumorigenic effects in vitro (**Figure S3I**). Hepa129 are widely used to establish orthotopic HCCs after injection into the liver of syngeneic C3H mice (42, 55). In this model, Y5R was confirmed to be strongly expressed by HCC cells also in vivo (**Figure S3J**), and pharmacologic Y5R-inhibition almost completely blocked in vivo tumor formation (**Figure 3E**; **Figure S3K**). In contrast, no toxic effects of pharmacologic Y5R-inhibition were detected in vivo and in vitro (**Figure S3L,M**). According to pharmacologic inhibition, RNAi-mediated specific Y5R-knockdown in Hepa129 cells (**Figure S3N**,**O**) confirmed marked reduction of in vivo tumor formation (**Figure 3F**) and growth (**Figure S3P-S**). Together, next to RNAi-mediated Y5R suppression, applying pharmacologic small molecule inhibitors identified this NPY-receptor as critical driver of HCC progression and as an attractive therapeutic target.

Neuropeptide Y is secreted by peri-tumorous hepatocytes and cross-talks with Y5-receptor in HCC

The strong effects of Y5R in HCC prompted us to further assess the role of its ligand NPY. We had hypothesized so far that serum-derived NPY (**Figure S2A**) is the major inductor of Y5R-activation. Unexpectedly, immunohistochemical analysis revealed marked NPY expression by tumor surrounding hepatocytes but only a weak staining signal in the majority of tumor cells in human HCC specimens (**Figure 4A**; **Figure S4A-**

C). In line with this, cultured human hepatocytes expressed and secreted NPY in approximately 10-fold higher amounts compared with HCC cells (**Figure 4B**,**C**). Also applying in vitro co-cultures and in the orthotopic HCC mouse model, we observed a striking contrast between pronounced NPY-expression in hepatocytes and absence of NPY-staining in HCC cells, while the receptor Y5R was exclusively and strongly expressed by HCC cells (**Figure 4D**,**E**; **Figure S4D**,**E**). Importantly, high peri-tumorous NPY expression in human liver tissues correlated with poor patient survival (**Figure 4F**; **Table S4**) and was associated with strong Y5-receptor expression by HCC cells (**Figure 4G**; **Table S2**). These data suggested that next to activation by serum-derived NPY, Y5R could drive liver cancer via direct cross-talk with hepatocyte-derived peri-tumorous NPY (**Figure S4F**).

Thus, we aimed to functionally verify this potential NPY-Y5R-interaction. In the previous functional in vitro experiments, NPY-containing serum had been added to the cell culture medium, and here, applying an NPY-neutralizing antibody significantly reduced the proliferation of HCC cells (**Figure 5A**). Furthermore, we now applied recombinant NPY to HCC cells in serum free medium. Previous studies showed that NPY-receptors depend on $G_{i/0}$-proteins and RAS-signaling thereby inducing MAPK-ERK and PI3K-AKT-pathway activation (56, 57). Here, we found that even high NPY doses (up to 1µM) did not affect AKT-activation in HCC cells (data not shown). However, recombinant NPY induced clonogenicity (**Figure 5B**) as well as ERK-activation in HCC cells applying low nanomolar concentrations (**Figure 5C**). Moreover, NPY-induced ERK-activation was completely blocked by co-treatment with a specific Y5R-inhibitor (**Figure 5C**). Likewise, the synthetic high-affinity Y5R-specific agonist "BWX46" (Y5R-Ago) (**Figure S4G**) strongly induced ERK-activation in HCC cells (**Figure 5D**). Following an additional approach, we performed co-culture-experiments with (NPY-producing) hepatocytes and HCC cells (**Figure S4H**). Here, we observed

significant inhibition of tumor cell proliferation after treatment with an Y5R-inhibitor or with an NPY-neutralizing antibody (**Figure 5E**). Furthermore, HCC cells treated with hepatocyte-derived (i.e. NPY-containing) supernatant (**Figure S4I**) showed strong Ki-67 expression and ERK-activation, which was significantly blocked by Y5R-inhibition (**Figure 5F**; **Figure S4J**).

Together, these data indicated peri-tumorous hepatocytes as so far unknown source of NPY and demonstrated that hepatocyte-derived NPY can drive liver cancer via cross-talk with Y5R on HCC cells.

Peri-tumorous NPY expression is induced by hepatic fibrosis and TGFβ-signaling

Next, we wanted to get insight into the underlying mechanisms that induce peri-tumorous NPY expression in liver cancer, which usually develops in chronic liver disease (2, 58). Immunohistological analysis of patient-derived tissues revealed that next to peri-tumorous hepatocytes, the strongest NPY-expression was detected around portal fields and fibrotic septa (**Figure 6A**,**B**; **Figure S5A**,**B**).

The activation of hepatic stellate cells (HSC) is the key event of hepatic fibrosis, with activated HSC being the major source of extracellular matrix expression and deposition (59, 60). Activation of HSC is characterized by expression of alpha-smooth muscle actin (α-SMA) and collagen type I expression (60). Quantitative RT-PCR analysis revealed a significant correlation between NPY and collagen expression in peri-tumorous liver tissues of HCC patients (**Figure 6C**). Moreover, next to its localization around portal fields and septa, NPY expression strongly correlated with liver fibrosis/cirrhosis (**Figure 6D**; **Table S4**). We observed that NPY-positive hepatocytes were closely localized to areas of HSC-activation (indicated by e.g. α-SMA expression) in peri-tumorous liver tissues (**Figure 6E**; **Figure S5C-E**; **Table S4**). Therefore, we

excluded that NPY could also be derived directly from HSC by applying ELISA and immunofluorescence analysis, revealing that NPY is exclusively expressed by hepatocytes both in vitro and in vivo (**Figure 7A**,**B**). Considering the striking co-localization of HSC-activation and NPY-immunopositive hepatocytes, we hypothesized that activated HSC may induce NPY expression in hepatocytes. In support of this, conditioned cell culture media from activated HSC induced NPY expression and protein secretion by hepatocytes (**Figure 7C**,**D**).

Activated HSC are a major cellular source of hepatic transforming growth factor-beta (TGFβ), which is known as one of the most important mediators of tissue fibrosis (60). Therefore, we used two model systems to investigate whether TGFβ could induce NPY expression in hepatocytes: i) cultured primary human hepatocytes (PHH) and ii) a hepatoblast-derived liver organoid model representing differentiated hepatocytes in a three-dimensional, in vivo-like system (61) (**Figure S6A**). In both of these models, TGFβ-treatment was confirmed to induce a dose-dependent upregulation of mesenchymal markers (62) (**Figure S6B**,**C**). Moreover, in both model systems, TGFβ-treatment strongly induced NPY expression in hepatocytes (**Figure 7E**,**F**). In vivo, immunohistological TGFβ-staining of human peri-tumorous liver tissues revealed strong expression in fibrotic septa (**Figure 7G**). Also hepatocytes localized close to the fibrotic septa revealed a positive TGFβ-immunosignal (**Figure 7G**). Herewith, TGFβ-staining strongly resembled the NPY expression pattern in peri-tumorous liver tissue. Accordingly, TGFβ expression was higher in peri-tumorous as compared to HCC tissues (**Figure 7H**,**I**) and significantly correlated with NPY expression in peri-tumorous liver tissue (**Figure 4H**,**J**; **Figure S6D**,**E**; **Table S4**).

Aiming to address this TGFβ-NPY-Y5R-cross-talk functionally, we established a hybrid-organoid model consisting of HCC cells and surrounding hepatocytes (**Figure S6F-H**). In this system, TGFβ induced ("peri-tumorous") NPY expression by

hepatocytes and enhanced HCC growth, which was blocked by Y5R-inhibition (**Figure S6I**,**J**).

Next to hepatic stellate cell activation, chronic liver damage is also associated with chronic inflammation (59, 60). Accordingly, we observed that - besides HSC-activation - the NPY expression of hepatocytes correlated with the number of infiltrating CD3-positive immune cells (**Figure S7A,B**; **Table S4,S5**). High CD3-positive immune cell infiltration also correlated with enhanced fibrosis and high α-SMA expression in peri-tumorous liver tissues and was also associated with reduced survival (**Figure S7B**; **Table S5**). We hypothesized that although activated HSC are considered to be a major cellular source of hepatic TGFβ (60), immune cells further contribute to (NPY-inducing) TGFβ-production in the HCC microenvironment. Moreover, further cytokines could affect NPY expression. Screening of several inflammatory cytokines that are known key drivers of chronic liver injury revealed strong correlation of IL-1β and IL-6 with NPY expression in peri-tumorous liver tissues (**Figure S7C**), while other cytokines including e.g. TNF-α (data not shown) showed no correlation with NPY expression. Treatment with recombinant IL-1β caused a moderate but significant increase of NPY-expression by hepatocytes **(Figure S7D**,**E**). In chronic liver disease, IL-1β is secreted both by activated hepatic stellate cells (63) and immune cells (64). In contrast to IL-1β, IL-6 treatment did not directly affect NPY expression (**Figure S7D**,**E**). However, IL-6 might indirectly promote NPY expression by induction of HSC-activation (65).

In summary, we found that hepatic fibrosis and inflammation induced hepatic NPY-induction and identified TGFβ as a novel major mediator of (hepatic) NPY expression. Our data further supported that TGFβ-induced NPY derived from (peri-tumorous) hepatocytes can drive liver cancer via cross-talk with Y5R.

Hepatocyte-derived NPY mediates chemotaxis via activation of Y5R

Besides the observed NPY effects on proliferation and clonogenicity of HCC cells, Y5R has also been described to have chemoattractive characteristics in bone marrow stem cells (66). Therefore, we hypothesized that the NPY-gradient induced by i) downregulation of NPY in HCC cells and ii) marked NPY expression by peri-tumorous hepatocytes could impact chemotaxis of HCC cells (**Figure 8A**). According to this hypothesis, high peri-tumorous NPY expression was shown to correlate with poor patient survival (**Figure 4F**), and TCGA data analysis revealed that low NPY expression in HCC was associated with high-risk patient cohorts and poor overall survival (**Figure S8A**). Applying real-time cell migration (xCELLigence) and Boyden chamber assays, recombinant NPY revealed strong dose-dependent chemoattractive features on HCC cells (**Figure 8B**,**C**; **Figure S8B**,**C**). Similarly, the specific Y5R-agonist (BWX46) acted as a strong chemoattractant for HCC cells (**Figure 8D**). In contrast, small molecule- and si-RNA-mediated Y5R-inhibition abrogated the chemotactic effects of NPY on HCC cells (**Figure 8E**,**F**; **Figure S8D**). Also hepatocyte-derived (i.e. NPY-containing) cell culture supernatants strongly induced chemotaxis of HCC cells (**Figure 8G**), and this inducing effect was markedly inhibited by co-treatment with a pharmacologic Y5R-inhibitor or by applying NPY-neutralizing antibodies (**Figure 8G**). The molecular link between MAPK-ERK-activation and chemotaxis is well-known in cancer (67). In line with this, we had found marked induction of ERK-signaling by NPY-Y5R-cross-talk between hepatocytes and HCC cells (**Figure 5C**,**D**,**F**). Moreover, strong ERK-activation of HCC cells was exclusively detected at the boarder of tumors in the orthotopic HCC model (i.e. the site of strong NPY expression by tumor-surrounding hepatocytes) (**Figure 8H**).

Next to ERK-activation, NPY-receptors can inhibit cAMP via activation of G_i-proteins (68). In contrast, induction of cAMP-signaling was shown to reduce HCC cell migration (69). Therefore, we hypothesized that NPY could mediate its pro-migratory/-

chemotactic effects also via Y5R-mediated cAMP-inhibition (in addition to ERK-induction). Bioluminescence resonance energy transfer (BRET) analysis revealed significant and dose-dependent inhibition of forskolin-induced cAMP-activation in HCC cells by NPY which was reduced by Y5R-inhibition (**Figure 8I**) as well as inhibition of forskolin-induced cAMP-activation by Y5R-agonist-treatment (**Figure 8J**). Functionally, the cAMP-inductor forskolin reduced migration of HCC cells which was (partly) rescued by both NPY and the Y5R-agonist BWX46 (**Figure 8K**). These data suggested that both NPY-Y5R-induced ERK-activation and cAMP-reduction promote chemotactic migration of HCC cells at tumor-parenchyma boarders. Moreover, immunohistochemical analysis of human HCC tissues revealed that enhanced peri-tumoral NPY-expression by hepatocytes was significantly associated with stromal invasion (Fisher's exact P = 0.001). In line with this, next to migration, NPY also induced chemotactic invasion of HCC cells (**Figure 8L**).

Together, these findings indicated that in addition to its effect on tumor growth, (peri-tumorous) NPY cross-talks with Y5R to induce chemotactic migration and might thereby drive invasion and dissemination of HCC cells.

TGFβ induces Y5R expression in HCC cells at sites of stroma-invasion

The strong effects of NPY on chemotaxis and invasion prompted us to further explore Y5R-expression at sites of stroma-invasion. At the invasive front, Y5R was even stronger expressed in HCC cells than in central tumor areas (**Figure 9A**). Moreover, immunohistochemical analysis revealed that enhanced Y5R expression significantly correlated with stromal invasion in human HCC (Fisher's exact: P = 0.041; Spearman correlation: R = 0.24; P = 0.007). In search for the underlying mechanisms, we considered TGFβ which was found to be highly expressed in the peri-tumorous regions (**Figure 7G-I**) and also in the invasive front together with Y5R (**Figure S9A**). In

addition, TGFβ is well known to play a critical role in the orchestration of invasion and the multistep epithelial-mesenchymal-transition (EMT)-process in different types of cancer including HCC (70, 71). Treatment of human HCC cells with recombinant TGFβ dose-dependently upregulated the expression of Y5R (**Figure 9B)** together with established EMT-markers (71) (**Figure S9B**).

Preliminary results from phase I/II clinical trials applying the specific TGFβ-receptor-1 (TGFBR1) inhibitor LY2157299 ("galunisertib") (**Figure S9C**) in HCC patients (ClinicalTrials.gov Identifiers: NCT01246986, NCT02906397, NCT02240433, NCT02178358, NCT02423343) have shown improved outcome and changes consistent with a reduction of EMT (72, 73). Here, we confirmed that galunisertib as well as a further specific TGFBR1-inhibitor (SB43152) (74) (**Figure S9D**) inhibited the TGFβ-induced expression of EMT-markers in human HCC cells (**Figure 9C**; **Figure S9E**). Importantly, both specific TGFBR1-inhibitors also completely prevented the TGFβ-mediated upregulation of Y5R in HCC cells as well as in HCC-HSC-co-cultures (**Figure 9D,E**; **Figure S9F,G**), indicating that TGFβ effects on Y5R expression of HCC cells are mediated via canonical and not via non-canonical TGFβ-signaling. Moreover, Y5R mRNA levels strongly correlated with TGFβ expression in HCC patient-derived tissue samples (**Figure 9F**), further supporting the impact of TGFβ-TGFBR1-signaling on Y5R expression of HCC cells.

Conversely, treatment with recombinant NPY or the specific Y5R-agonist induced SNAIL expression in HCC cells (**Figure S9H**). Moreover, we found that incubation with NPY or the specific Y5R-agonist also induced chemokinetic (i.e. non-directed) migration of HCC cells via Y5R-activation (**Figure 9G**; **Figure S9I**) in addition to the above described chemoattractive effects. Therefore, considering the strong local co-expression of TGFβ, Y5R and NPY at sites of stroma invasion, TGFβ might promote HCC cell dissemination (75) by activation of the Y5R-NPY-axis. Accordingly, Boyden

chamber assays confirmed that pre-treatment with TGFβ induced the migratory activity of HCC cells which was completely blocked by Y5R-inhibition (**Figure 9H**). Considering these findings, we hypothesized that TGFβ might also (co)-regulate the age-dependent Y5R expression that we had observed in the experimental C3H mouse model and in liver tissues of HCC patients (**Figure 1**; **Figure S1**). However, we found that neither in in C3H mice nor in human tissues, TGFβ correlated (positively) with age or with age-associated Y5R expression, respectively (**Figure S9J-L**).

In summary, these findings indicated that TGFβ is not only a so far unknown inducer of (hepatic) NPY expression but also promotes the expression of the NPY-receptor Y5R in cancer cells at the site of stromal invasion via activation of the canonical TGFβ-TGFBR1/2-dependent pathway. Moreover, our data suggest that at least part of the TGFβ-TGFBR1/2-signaling mediated effect on EMT and stroma-invasion is mediated via Y5R-activation.

Y5R-activation is augmented by dipeptidylpeptidase 4 overexpression in HCC

In contrast to Y5R, the Y1- and Y2-receptor subtypes were not regulated by TGFβ-signaling (data not shown). Furthermore, YR1 and YR2 were not overexpressed in murine and human HCC and revealed no oncogenic functions in liver cancer (**Figure S10A-S**). Therefore, Y5R was identified to be the only NPY-receptor that serves as a potent candidate oncogenic target in liver cancer.

The so called "NPY-converting enzyme" dipeptidylpeptidase-4 (DPP4) is a cell surface enzyme which has also a soluble form. DPP4 terminates the Y1R-activity of NPY by cleaving Tyr_1 and Pro_2 from $NPY_{1\text{-}36}$ to form $NPY_{3\text{-}36}$, which more specifically activates Y5R (76, 77). Just recently, it has been described that hepatocytes secrete DPP4 and herewith promote insulin resistance and adipose tissue inflammation in obese patients (78). We therefore asked whether DPP4-induced "NPY-conversion" to Y5R-specific

$NPY_{3\text{-}36}$ might contribute to Y5R-mediated HCC progression. We found that DPP4 expression levels were markedly increased in human HCC cell lines compared with poor expression in hepatocytes (**Figure 10A**). Also applying several patient-derived datasets including TCGA-data as well as in our patient-derived samples, we detected a strong overexpression of DPP4 levels in HCC tissues as compared with (corresponding) non-tumorous liver tissue (**Figure 7B-D**). In hepatocytes, DPP4 was described to be mainly localized on the bile canalicular surface (79). We detected a similar distribution of DPP4-immonoreactivity in peri-tumorous patient tissues and strong expression in most HCC tissues. In some tumor tissues (but not in non-tumorous liver tissues), the HCC cells revealed strong DPP4-expression on the entire cell membrane, which could be explained by a loss of polarity of cancer cells (**Figure 10E**; **Figure S11A**). Confirming in vitro, in silico and in vivo analysis of DPP4 (mRNA) expression levels, DPP4-immunoreactivity revealed strongly enhanced protein expression in most HCC tissues as compared with non-tumorous liver tissue (**Figure 10E**,**F**; **Figure S11A**). In line with these data, potential interaction of DPP4 with the NPY-Y5R-axis in HCC was supported by strong correlation of DPP4 and Y5R expression levels in HCC patient-derived tissue samples (**Figure S11A**,**B**) as well as by co-upregulation of DPP4 and Y5R mRNA expression in HCC compared with corresponding non-tumorous tissues (**Figure S11C**). High DPP4 protein expression in HCC cells also correlated with peri-tumorous NPY expression (**Table S6**). Analysis of a TCGA-derived HCC patient cohort revealed that high expression of DPP4 by itself showed a (non-significant) trend towards correlation with poor survival (**Figure S11D**). However, combined elevated tumorous DPP4 and Y5R expression together with enhanced peri-tumorous NPY expression was significantly correlated with poor HCC patient survival (**Figure S11E**). Together, these data supported that NPY derived from

peri-tumorous hepatocytes could be locally converted by DPP4 to enhance Y5R-activation and receptor-subtype-specificity to drive liver cancer.

Based on these findings and hypotheses, we aimed to functionally analyze the impact of DPP4-inhibition on the pro-tumorigenic action of Y5R in HCC cells. Therefore, RNAi-mediated specific knockdown of DPP4 was performed in HCC cells (**Figure S11F**). Applying serum-supplemented (i.e. NPY-containing) culture media, subsequent analysis revealed strong reduction of both clonogenicity (**Figure 11A**) and proliferation (**Figure 11B**) of HCC cells after DPP4-knockdown. In contrast, Boyden chamber analysis of migration applying serum-free (i.e. without NPY) culture media as a chemoattractant showed no effect of DPP4-knockout, while enhanced chemotaxis mediated by recombinant NPY was prevented by combined DPP4-knockout (**Figure 11C**).

Besides NPY, DPP4 cleaves glucagon-like peptide 1 (GLP-1) which is strongly involved in glucose metabolism. Therefore, orally administered specific DPP4-inhibitors like sitagliptin (**Figure S11G**) have become clinically successful standard therapeutic agents for type 2 diabetes (80). Here, we used sitagliptin to confirm the effects of DPP4-knockout on NPY-mediated Y5R-activation as well as to analyze the use of "gliptins" as a potential pharmacologic application to target the DPP4-NPY-Y5R-axis in HCC. Sitagliptin dose-dependently reduced proliferation of HCC cells in serum (i.e. NPY)-containing culture medium (**Figure S11H**), and this inhibitory effect was rescued by the specific Y5R-agonist "BWX46" (**Figure 11D**). Moreover, NPY-induced chemotaxis of HCC cells was significantly reduced by sitagliptin (**Figure 11E**). In contrast, sitagliptin did not affect chemotaxis-induction by the specific Y5R-agonist ("BWX46") which has no DPP4-cleavage-site (**Figure 11F**).

Together, these data indicated that Y5R-stimulation in HCC is promoted by DPP4-induced NPY-conversion to truncated $NPY_{3\text{-}36}$ which terminates Y1R- and augments

Y5R-specificity (**Figure 11G**). Our findings suggest DPP4-inhibition using clinically established drugs as a further promising therapeutic strategy to target the newly identified NPY-Y5R-axis in HCC.

DISCUSSION

Numerous studies suggested that the NPY-system might play a critical role in aging and lifespan as well as in further cancer-related hallmarks (17, 19-24, 51). Hypothalamic NPY levels decrease in aged animals (18), and a reduced cerebral NPY production could contribute to altered reproductive function and food intake in aged subjects (81). In contrast, activation of the NPY-system was shown in several human disorders including chronic liver disease (25, 26, 82) as well as hepatic glucose (29) and lipid (30) metabolism, but its potential role in liver cancer was unknown.

In this study, we found that the expression of the Y5-NPY-receptor (Y5R) in peri-tumorous liver tissues increased with age both in a mouse model and in patients. This might reflect a compensatory upregulation of Y5R due to low systemic levels of its ligand NPY in aged humans (83). Furthermore, it might result from age-related alterations of methylation of the Y5R promotor. After malignant transformation, HCC cells take advantage from a further upregulation of Y5R expression, which is induced by microenvironment-derived factors including TGFβ. Moreover, in addition to systemic serum derived NPY, Y5R gets activated via cross-talk with local NPY derived from peri-tumorous hepatocytes.

Deciphering the underlying mechanisms of peri-tumorous NPY secretion by hepatocytes, we revealed that hepatic fibrosis contributes to NPY-induction and identified TGFβ-TGFBR1-signaling as a major novel mediator of NPY expression by hepatocytes. Strikingly, TGFβ is considered to be a potent modulator of fibrosis and HCC development (84-86).

Conversely, we found that non-Y5-NPY-receptors (Y1R and Y2R) were downregulated and did not have tumor promoting functions in HCC. Actually, Y1R even revealed suppressive effects on tumor cell migration, which is in accordance with the only study

that investigated the potential function of a NPY-receptor in liver cancer so far (87). In line with our findings, Lv et al. observed that Y1R is downregulated in HCC and that forced overexpression of Y1R mediates tumor suppressor functions in HCC cells (87). In contrast to this single study on Y1R function, the potential roles of NPY, Y2R and Y5R in HCC had been entirely unknown. Here, we show for the first time that the NPY-Y5R-axis mediates proliferation, stemness-associated properties, chemotactic migration and invasion in liver cancer. A previous study found that stimulation of the Y1-receptor could induce TGFβ secretion by macrophages and herewith affected neuroprotection and hematopoietic stem cell survival in the bone marrow (88). However, to the best of our knowledge, a (converse) regulation of the NPY-system by TGFβ has not yet been described.

Here, we revealed that NPY expression in hepatocytes and Y5R expression in HCC cells, respectively, are regulated via TGFβ-TGFBR1-signaling. Furthermore, our study indicated that TGFβ-mediated effects on HCC tumorigenicity are at least in part mediated by Y5R activation. Besides canonical (TGFBR1-dependent) signaling, TGFβ can also activate Smad1/5/8 (i.e. BMP-associated) pathways through Activin Receptor-Like Kinase 1 (ALK1) together with TGFBR2 (89). Indeed, ALK1-dependent signaling represents a potential alternative mechanism of TGFβ-signaling in HCC and the ALK1-inhibitor dalantercept is currently investigated in clinical trials in HCC patients (90). However, our study provides mechanistic evidence that the effects of TGFβ-signaling on the NPY-Y5R-axis in HCC are mediated via the canonical, TGFBR1-related pathway. Therefore, pharmacologic inhibition of the TGFβ-TGFBR1-axis might represent a potential strategy to target the NPY-Y5R-axis in HCC.

We further found that the NPY-converting enzyme DPP4 is upregulated in HCC and augments Y5R function. DPP4 was recently linked to aging and has been shown to be involved in age-dependent dysfunction of bone and hematopoietic regeneration (91).

Moreover, a recent study reported that hepatocyte-secreted DPP4 in obesity promotes adipose inflammation and insulin resistance (78), further promoting the value of clinically established DPP4-inhibition for the treatment of (different components) of the metabolic syndrome and its complications. Here, we found that Y5R-stimulation in HCC is promoted by DPP4-induced NPY-conversion which terminates Y1R- and augments Y5R-specificity. Thus, our study suggests that next to direct targeting of Y5R or the TGFβ-TGFBR1-NPY-Y5R axis, DPP4-inhibition might represent a further attractive therapeutic strategy for controlling liver cancer.

Regarding potential further therapeutic applications, we revealed that the NPY-Y5R-axis activates MAPK-ERK-signaling. Therefore, future studies could examine if Y5R might contribute to efficacy and/or therapy resistance of current first-line therapeutic options for advanced HCC (e.g. sorafenib) that are known to target the RAF-ERK-axis.

In summary, targeting the TGFβ-NPY-DPP4-Y5R axis could represent a novel therapeutic avenue in HCC and also other types of cancer.

EXPERIMENTAL PROCEDURES

Animal models

Eighteen months old male C3H/HeN mice were used as a model system of age-related spontaneous hepatocarcinogenesis as described (32-38). A murine orthotopic HCC allograft model (42) was used to analyze the therapeutic effect of the specific small molecule Y5R-inhibitor "CGP71683" (52) as well as the effect of RNAi-mediated Y5R-knockout. Animals were obtained from Charles River Laboratories (Sulzfeld, Germany) and housed under specific pathogen-free and controlled conditions.

Human cells and tissues

Pairs of human HCC tissues and corresponding non-tumorous liver tissues were obtained from patients after partial hepatectomy. Informed consent was obtained through the Human Tissue and Cell Research (HTCR) foundation (92). The samples were immediately snap-frozen and stored at -80°C.

The tissue micro array (TMA) consisted of paired HCC and corresponding non-neoplastic liver tissues which were obtained from HCC patients undergoing surgical resection and was previously described (42).

Statistical analysis

Results were expressed as mean ± SEM. Comparison between groups was made using the 2-tailed Student’s t-test or one-way ANOVA together with Dunnett′s multiple comparisons test, if appropriate. Spearman and Pearson correlation coefficients, respectively, were used for correlation analysis. Analysis of tissue micro arrays was performed using the Fisher’s exact test, Spearman correlation analysis as well as uni- and multivariate analysis applying the SPSS ordinal regression procedure ("PLUM";

Polytomous Universal Model; link function: logit). In silico survival analysis were performed computationally applying Log-rank testing and Hazard ratio estimates. A P-value less than 0.05 ($P < 0.05$) was considered significant. The level of significance was depicted in figures as *$P < 0.05$, **$P < 0.01$, ***$P < 0.001$ and ****$P < 0.0001$ or "ns", i.e. non-significant. The number of experiments is depicted in figure legends. Calculations were performed using the GraphPad Prism Software (GraphPad Software, Inc., San Diego, CA, USA) and SPSS (SPSS Statistics 23, IBM Corp., USA).

Study approval

The animal studies were approved by the Committee for Animal Health and Care of the local government (RUF-55.2.2-2532-2-566-11), and conformed to international guidelines on the ethical use of animals.

Patients signed an informed consent in accordance with the Helsinki declaration before being enrolled in the study. The Biobank at Hospital of the Ludwig-Maximilians-University Munich (HTCR) is under administration of the non-profit state-controlled HTCR Foundation, following ethical approval (LMU Munich, No. 25-12).

More-detailed procedures can be found in supplemental experimental procedures.

AUTHOR CONTRIBUTIONS:

P.D., A.K.B., and C.H. conceived the project, analyzed the data, and wrote the paper. P.D., L.W., V.F., T.S., M.D.M., A.S., C.G., T.I., A.T. and C.G. designed and performed the experiments. A.E.K., W.E.T., J.T., A.H., M.F.N., S.v.H., A.K.B. and C.H. provided material and contributed to data analysis and manuscript creation, respectively.

ACKNOWLEDGEMENTS:

This work was supported by grants from the German Research Association (DFG) (Research Training Group "RTG 1962/1" and FOR 2127 to PD, AB and CH), the German Cancer Aid (Deutsche Krebshilfe to PD and AB), the Bavarian Research Network for Molecular Biosystems (BioSysNet; to AB), the Else-Kröner-Fresenius Stiftung (EKFS, to PD), and the Interdisciplinary Center for Clinical Research (IZKF) Erlangen (to PD, AB and CH). We would like to thank Reiner Wiest (Inselspital, Bern, Switzerland) for valuable suggestions and critical discussion of the manuscript. We thank Annette Serwotka, Darleen Schönwälder, Sabrina Freitag, Manuel Munz and Rudolph Jung for excellent technical assistance.

We acknowledge the Human Tissue and Cell Research foundation (HTCR, Regensburg, Germany) for making human tissue available for research, as well as Hepacult GmbH (Planegg / Martinsried, Germany) for providing primary human hepatocytes for in vitro studies. We appreciate the provision of suitable samples by the Biobank under administration of HTCR at the Hospital of the Ludwig-Maximilians-University Munich based on extensive data and sample analysis.

REFERENCES

1. Yang JD, Hainaut P, Gores GJ, Amadou A, Plymoth A, and Roberts LR. A global view of hepatocellular carcinoma: trends, risk, prevention and management. *Nat Rev Gastroenterol Hepatol.* 2019;16(10):589-604.
2. Dietrich P, and Hellerbrand C. Non-alcoholic fatty liver disease, obesity and the metabolic syndrome. *Best Pract Res Clin Gastroenterol.* 2014;28(4):637-53.
3. El-Serag HB, and Rudolph KL. Hepatocellular carcinoma: epidemiology and molecular carcinogenesis. *Gastroenterology.* 2007;132(7):2557-76.
4. de Magalhaes JP. How ageing processes influence cancer. *Nat Rev Cancer.* 2013;13(5):357-65.
5. Peto J. Cancer epidemiology in the last century and the next decade. *Nature.* 2001;411(6835):390-5.
6. Hanahan D, and Weinberg RA. Hallmarks of cancer: the next generation. *Cell.* 2011;144(5):646-74.
7. Lopez-Otin C, Blasco MA, Partridge L, Serrano M, and Kroemer G. The hallmarks of aging. *Cell.* 2013;153(6):1194-217.
8. Ziegler MG, Lake CR, and Kopin IJ. Plasma noradrenaline increases with age. *Nature.* 1976;261(5558):333-5.
9. Seals DR, and Esler MD. Human ageing and the sympathoadrenal system. *J Physiol.* 2000;528(Pt 3):407-17.
10. Renz BW, Takahashi R, Tanaka T, Macchini M, Hayakawa Y, Dantes Z, et al. beta2 Adrenergic-Neurotrophin Feedforward Loop Promotes Pancreatic Cancer. *Cancer Cell.* 2018;33(1):75-90 e7.
11. Thaker PH, Han LY, Kamat AA, Arevalo JM, Takahashi R, Lu C, et al. Chronic stress promotes tumor growth and angiogenesis in a mouse model of ovarian carcinoma. *Nat Med.* 2006;12(8):939-44.
12. Magnon C, Hall SJ, Lin J, Xue X, Gerber L, Freedland SJ, et al. Autonomic nerve development contributes to prostate cancer progression. *Science.* 2013;341(6142):1236361.
13. Li J, Yang XM, Wang YH, Feng MX, Liu XJ, Zhang YL, et al. Monoamine oxidase A suppresses hepatocellular carcinoma metastasis by inhibiting the adrenergic system and its transactivation of EGFR signaling. *J Hepatol.* 2014;60(6):1225-34.
14. Hirsch D, and Zukowska Z. NPY and stress 30 years later: the peripheral view. *Cell Mol Neurobiol.* 2012;32(5):645-59.
15. Clarke J, Benjamin N, Larkin S, Webb D, Maseri A, and Davies G. Interaction of neuropeptide Y and the sympathetic nervous system in vascular control in man. *Circulation.* 1991;83(3):774-7.
16. Yi M, Li H, Wu Z, Yan J, Liu Q, Ou C, et al. A Promising Therapeutic Target for Metabolic Diseases: Neuropeptide Y Receptors in Humans. *Cell Physiol Biochem.* 2018;45(1):88-107.
17. Botelho M, and Cavadas C. Neuropeptide Y: An Anti-Aging Player? *Trends Neurosci.* 2015;38(11):701-11.
18. Aveleira CA, Botelho M, Carmo-Silva S, Pascoal JF, Ferreira-Marques M, Nobrega C, et al. Neuropeptide Y stimulates autophagy in hypothalamic neurons. *Proc Natl Acad Sci U S A.* 2015;112(13):E1642-51.
19. Yang Y, Atasoy D, Su HH, and Sternson SM. Hunger states switch a flip-flop memory circuit via a synaptic AMPK-dependent positive feedback loop. *Cell.* 2011;146(6):992-1003.
20. Marsh DJ, Hollopeter G, Kafer KE, and Palmiter RD. Role of the Y5 neuropeptide Y receptor in feeding and obesity. *Nat Med.* 1998;4(6):718-21.
21. Minor RK, Lopez M, Younts CM, Jones B, Pearson KJ, Anson RM, et al. The arcuate nucleus and neuropeptide Y contribute to the antitumorigenic effect of calorie restriction. *Aging Cell.* 2011;10(3):483-92.
22. Kallio J, Pesonen U, Kaipio K, Karvonen MK, Jaakkola U, Heinonen OJ, et al. Altered intracellular processing and release of neuropeptide Y due to leucine 7 to proline 7

polymorphism in the signal peptide of preproneuropeptide Y in humans. *Faseb J.* 2001;15(7):1242-4.
23. Hansel DE, Eipper BA, and Ronnett GV. Neuropeptide Y functions as a neuroproliferative factor. *Nature.* 2001;410(6831):940-4.
24. Singh P, Hoggatt J, Kamocka MM, Mohammad KS, Saunders MR, Li H, et al. Neuropeptide Y regulates a vascular gateway for hematopoietic stem and progenitor cells. *J Clin Invest.* 2017.
25. Moleda L, Trebicka J, Dietrich P, Gabele E, Hellerbrand C, Straub RH, et al. Amelioration of portal hypertension and the hyperdynamic circulatory syndrome in cirrhotic rats by neuropeptide Y via pronounced splanchnic vasoaction. *Gut.* 2011;60(8):1122-32.
26. Dietrich P, Moleda L, Kees F, Muller M, Straub RH, Hellerbrand C, et al. Dysbalance in sympathetic neurotransmitter release and action in cirrhotic rats: impact of exogenous neuropeptide Y. *J Hepatol.* 2013;58(2):254-61.
27. Hartl J, Dietrich P, Moleda L, Muller-Schilling M, and Wiest R. Neuropeptide Y restores non-receptor-mediated vasoconstrictive action in superior mesenteric arteries in portal hypertension. *Liver Int.* 2015;35(12):2556-63.
28. Sigala B, McKee C, Soeda J, Pazienza V, Morgan M, Lin CI, et al. Sympathetic nervous system catecholamines and neuropeptide Y neurotransmitters are upregulated in human NAFLD and modulate the fibrogenic function of hepatic stellate cells. *PLoS One.* 2013;8(9):e72928.
29. Li L, de La Serre CB, Zhang N, Yang L, Li H, and Bi S. Knockdown of Neuropeptide Y in the Dorsomedial Hypothalamus Promotes Hepatic Insulin Sensitivity in Male Rats. *Endocrinology.* 2016;157(12):4842-52.
30. Ailanen L, Ruohonen ST, Vahatalo LH, Tuomainen K, Eerola K, Salomaki-Myftari H, et al. The metabolic syndrome in mice overexpressing neuropeptide Y in noradrenergic neurons. *J Endocrinol.* 2017;234(1):57-72.
31. Bruinstroop E, Pei L, Ackermans MT, Foppen E, Borgers AJ, Kwakkel J, et al. Hypothalamic neuropeptide Y (NPY) controls hepatic VLDL-triglyceride secretion in rats via the sympathetic nervous system. *Diabetes.* 2012;61(5):1043-50.
32. Becker FF. Inhibition of spontaneous hepatocarcinogenesis in C3H/HeN mice by transplanted hepatocellular carcinomas. *Cancer Res.* 1981;41(9 Pt 1):3320-3.
33. Becker FF, Stillman D, and Sell S. Serum alpha-fetoprotein in a mouse strain (C3H-Avy fB) with spontaneous hepatocellular carcinomas. *Cancer Res.* 1977;37(3):870-2.
34. Heston WE, Vlahakis G, and Deringer MK. High incidence of spontaneous hepatomas and the increase of this incidence with urethan in C3H, C3Hf, and C3He male mice. *J Natl Cancer Inst.* 1960;24:425-35.
35. Buchmann A, Bauer-Hofmann R, Mahr J, Drinkwater NR, Luz A, and Schwarz M. Mutational activation of the c-Ha-ras gene in liver tumors of different rodent strains: correlation with susceptibility to hepatocarcinogenesis. *Proc Natl Acad Sci U S A.* 1991;88(3):911-5.
36. Jang JJ, Weghorst CM, Henneman JR, Devor DE, and Ward JM. Progressive atypia in spontaneous and N-nitrosodiethylamine-induced hepatocellular adenomas of C3H/HeNCr mice. *Carcinogenesis.* 1992;13(9):1541-7.
37. Lee GH, Sawada N, Mochizuki Y, Nomura K, and Kitagawa T. Immortal epithelial cells of normal C3H mouse liver in culture: possible precursor populations for spontaneous hepatocellular carcinoma. *Cancer Res.* 1989;49(2):403-9.
38. Ruebner BH, Gershwin ME, Meierhenry EF, Hsieh LS, and Dunn PL. Irreversibility of liver tumors in C3H mice. *J Natl Cancer Inst.* 1984;73(2):493-8.
39. Wolf MJ, Adili A, Piotrowitz K, Abdullah Z, Boege Y, Stemmer K, et al. Metabolic activation of intrahepatic CD8+ T cells and NKT cells causes nonalcoholic steatohepatitis and liver cancer via cross-talk with hepatocytes. *Cancer Cell.* 2014;26(4):549-64.
40. Chaisaingmongkol J, Budhu A, Dang H, Rabibhadana S, Pupacdi B, Kwon SM, et al. Common Molecular Subtypes Among Asian Hepatocellular Carcinoma and Cholangiocarcinoma. *Cancer Cell.* 2017;32(1):57-70 e3.

41. Llovet JM, Burroughs A, and Bruix J. Hepatocellular carcinoma. *Lancet.* 2003;362(9399):1907-17.
42. Dietrich P, Koch A, Fritz V, Hartmann A, Bosserhoff AK, and Hellerbrand C. Wild type Kirsten rat sarcoma is a novel microRNA-622-regulated therapeutic target for hepatocellular carcinoma and contributes to sorafenib resistance. *Gut.* 2017.
43. Hellerbrand C, Amann T, Schlegel J, Wild P, Bataille F, Spruss T, et al. The novel gene MIA2 acts as a tumour suppressor in hepatocellular carcinoma. *Gut.* 2008;57(2):243-51.
44. Amann T, Bataille F, Spruss T, Dettmer K, Wild P, Liedtke C, et al. Reduced expression of fibroblast growth factor receptor 2IIIb in hepatocellular carcinoma induces a more aggressive growth. *Am J Pathol.* 2010;176(3):1433-42.
45. Huang WY, Hsu SD, Huang HY, Sun YM, Chou CH, Weng SL, et al. MethHC: a database of DNA methylation and gene expression in human cancer. *Nucleic Acids Res.* 2015;43(Database issue):D856-61.
46. Perez RF, Tejedor JR, Bayon GF, Fernandez AF, and Fraga MF. Distinct chromatin signatures of DNA hypomethylation in aging and cancer. *Aging Cell.* 2018;17(3):e12744.
47. Mudbhary R, Hoshida Y, Chernyavskaya Y, Jacob V, Villanueva A, Fiel MI, et al. UHRF1 overexpression drives DNA hypomethylation and hepatocellular carcinoma. *Cancer Cell.* 2014;25(2):196-209.
48. Barcena-Varela M, Caruso S, Llerena S, Alvarez-Sola G, Uriarte I, Latasa MU, et al. Dual Targeting of Histone Methyltransferase G9a and DNA-Methyltransferase 1 for the Treatment of Experimental Hepatocellular Carcinoma. *Hepatology.* 2019;69(2):587-603.
49. Argemi J, Latasa MU, Atkinson SR, Blokhin IO, Massey V, Gue JP, et al. Defective HNF4alpha-dependent gene expression as a driver of hepatocellular failure in alcoholic hepatitis. *Nat Commun.* 2019;10(1):3126.
50. Yamashita T, and Wang XW. Cancer stem cells in the development of liver cancer. *J Clin Invest.* 2013;123(5):1911-8.
51. Nakamura Y, Yanagawa Y, Morrison SF, and Nakamura K. Medullary Reticular Neurons Mediate Neuropeptide Y-Induced Metabolic Inhibition and Mastication. *Cell Metab.* 2017;25(2):322-34.
52. Criscione L, Rigollier P, Batzl-Hartmann C, Rueger H, Stricker-Krongrad A, Wyss P, et al. Food intake in free-feeding and energy-deprived lean rats is mediated by the neuropeptide Y5 receptor. *J Clin Invest.* 1998;102(12):2136-45.
53. Turnbull AV, Ellershaw L, Masters DJ, Birtles S, Boyer S, Carroll D, et al. Selective antagonism of the NPY Y5 receptor does not have a major effect on feeding in rats. *Diabetes.* 2002;51(8):2441-9.
54. Erondu N, Gantz I, Musser B, Suryawanshi S, Mallick M, Addy C, et al. Neuropeptide Y5 receptor antagonism does not induce clinically meaningful weight loss in overweight and obese adults. *Cell Metab.* 2006;4(4):275-82.
55. Schmitz V, Tirado-Ledo L, Tiemann K, Raskopf E, Heinicke T, Ziske C, et al. Establishment of an orthotopic tumour model for hepatocellular carcinoma and non-invasive in vivo tumour imaging by high resolution ultrasound in mice. *J Hepatol.* 2004;40(5):787-91.
56. Mannon PJ, and Raymond JR. The neuropeptide Y/peptide YY Y1 receptor is coupled to MAP kinase via PKC and Ras in CHO cells. *Biochem Biophys Res Commun.* 1998;246(1):91-4.
57. Mullins DE, Zhang X, and Hawes BE. Activation of extracellular signal regulated protein kinase by neuropeptide Y and pancreatic polypeptide in CHO cells expressing the NPY Y(1), Y(2), Y(4) and Y(5) receptor subtypes. *Regul Pept.* 2002;105(1):65-73.
58. Nakagawa S, Wei L, Song WM, Higashi T, Ghoshal S, Kim RS, et al. Molecular Liver Cancer Prevention in Cirrhosis by Organ Transcriptome Analysis and Lysophosphatidic Acid Pathway Inhibition. *Cancer Cell.* 2016;30(6):879-90.
59. Tsuchida T, and Friedman SL. Mechanisms of hepatic stellate cell activation. *Nat Rev Gastroenterol Hepatol.* 2017;14(7):397-411.

60. Bataller R, and Brenner DA. Liver fibrosis. *J Clin Invest.* 2005;115(2):209-18.
61. Saito Y, Nakaoka T, Muramatsu T, Ojima H, Sukeda A, Sugiyama Y, et al. Induction of differentiation of intrahepatic cholangiocarcinoma cells to functional hepatocytes using an organoid culture system. *Sci Rep.* 2018;8(1):2821.
62. Nitta T, Kim JS, Mohuczy D, and Behrns KE. Murine cirrhosis induces hepatocyte epithelial mesenchymal transition and alterations in survival signaling pathways. *Hepatology.* 2008;48(3):909-19.
63. Ruddell RG, Hoang-Le D, Barwood JM, Rutherford PS, Piva TJ, Watters DJ, et al. Ferritin functions as a proinflammatory cytokine via iron-independent protein kinase C zeta/nuclear factor kappaB-regulated signaling in rat hepatic stellate cells. *Hepatology.* 2009;49(3):887-900.
64. Kubes P, and Mehal WZ. Sterile inflammation in the liver. *Gastroenterology.* 2012;143(5):1158-72.
65. Xiang DM, Sun W, Ning BF, Zhou TF, Li XF, Zhong W, et al. The HLF/IL-6/STAT3 feedforward circuit drives hepatic stellate cell activation to promote liver fibrosis. *Gut.* 2018;67(9):1704-15.
66. Park MH, Lee JK, Kim N, Min WK, Lee JE, Kim KT, et al. Neuropeptide Y Induces Hematopoietic Stem/Progenitor Cell Mobilization by Regulating Matrix Metalloproteinase-9 Activity Through Y1 Receptor in Osteoblasts. *Stem Cells.* 2016;34(8):2145-56.
67. Vial E, Sahai E, and Marshall CJ. ERK-MAPK signaling coordinately regulates activity of Rac1 and RhoA for tumor cell motility. *Cancer Cell.* 2003;4(1):67-79.
68. Fredholm BB, Jansen I, and Edvinsson L. Neuropeptide Y is a potent inhibitor of cyclic AMP accumulation in feline cerebral blood vessels. *Acta Physiol Scand.* 1985;124(3):467-9.
69. Mukai M, Nakamura H, Tatsuta M, Iwasaki T, Togawa A, Imamura F, et al. Hepatoma cell migration through a mesothelial cell monolayer is inhibited by cyclic AMP-elevating agents via a Rho-dependent pathway. *FEBS Lett.* 2000;484(2):69-73.
70. Giannelli G, Koudelkova P, Dituri F, and Mikulits W. Role of epithelial to mesenchymal transition in hepatocellular carcinoma. *J Hepatol.* 2016;65(4):798-808.
71. Krebs AM, Mitschke J, Lasierra Losada M, Schmalhofer O, Boerries M, Busch H, et al. The EMT-activator Zeb1 is a key factor for cell plasticity and promotes metastasis in pancreatic cancer. *Nat Cell Biol.* 2017;19(5):518-29.
72. Giannelli G, Villa E, and Lahn M. Transforming growth factor-beta as a therapeutic target in hepatocellular carcinoma. *Cancer Res.* 2014;74(7):1890-4.
73. Rani B, Malfettone A, Dituri F, Soukupova J, Lupo L, Mancarella S, et al. Galunisertib suppresses the staminal phenotype in hepatocellular carcinoma by modulating CD44 expression. *Cell Death Dis.* 2018;9(3):373.
74. Matsuyama S, Iwadate M, Kondo M, Saitoh M, Hanyu A, Shimizu K, et al. SB-431542 and Gleevec inhibit transforming growth factor-beta-induced proliferation of human osteosarcoma cells. *Cancer Res.* 2003;63(22):7791-8.
75. Coulouarn C, Factor VM, and Thorgeirsson SS. Transforming growth factor-beta gene expression signature in mouse hepatocytes predicts clinical outcome in human cancer. *Hepatology.* 2008;47(6):2059-67.
76. Zukowska-Grojec Z, Karwatowska-Prokopczuk E, Rose W, Rone J, Movafagh S, Ji H, et al. Neuropeptide Y: a novel angiogenic factor from the sympathetic nerves and endothelium. *Circ Res.* 1998;83(2):187-95.
77. Wagner L, Kaestner F, Wolf R, Stiller H, Heiser U, Manhart S, et al. Identifying neuropeptide Y (NPY) as the main stress-related substrate of dipeptidyl peptidase 4 (DPP4) in blood circulation. *Neuropeptides.* 2016;57:21-34.
78. Ghorpade DS, Ozcan L, Zheng Z, Nicoloro SM, Shen Y, Chen E, et al. Hepatocyte-secreted DPP4 in obesity promotes adipose inflammation and insulin resistance. *Nature.* 2018;555(7698):673-7.
79. Fukui Y, Yamamoto A, Kyoden T, Kato K, and Tashiro Y. Quantitative immunogold localization of dipeptidyl peptidase IV (DPP IV) in rat liver cells. *Cell Struct Funct.* 1990;15(2):117-25.

80. Drucker DJ, and Nauck MA. The incretin system: glucagon-like peptide-1 receptor agonists and dipeptidyl peptidase-4 inhibitors in type 2 diabetes. *Lancet.* 2006;368(9548):1696-705.
81. Gruenewald DA, Naai MA, Marck BT, and Matsumoto AM. Age-related decrease in neuropeptide-Y gene expression in the arcuate nucleus of the male rat brain is independent of testicular feedback. *Endocrinology.* 1994;134(6):2383-9.
82. Wiest R, Jurzik L, Moleda L, Froh M, Schnabl B, von Horsten S, et al. Enhanced Y1-receptor-mediated vasoconstrictive action of neuropeptide Y (NPY) in superior mesenteric arteries in portal hypertension. *J Hepatol.* 2006;44(3):512-9.
83. Chiodera P, Volpi R, Pilla S, Cataldo S, and Coiro V. Decline in circulating neuropeptide Y levels in normal elderly human subjects. *Eur J Endocrinol.* 2000;143(5):715-6.
84. Delire B, Lebrun V, Selvais C, Henriet P, Bertrand A, Horsmans Y, et al. Aging enhances liver fibrotic response in mice through hampering extracellular matrix remodeling. *Aging (Albany NY).* 2016;9(1):98-113.
85. Richter K, Konzack A, Pihlajaniemi T, Heljasvaara R, and Kietzmann T. Redox-fibrosis: Impact of TGFbeta1 on ROS generators, mediators and functional consequences. *Redox Biol.* 2015;6:344-52.
86. Arrese M, Cabrera D, Hernandez A, Astete L, Estrada L, and Cabello-Verrugio C. TGF-beta and Hepatocellular Carcinoma: When A Friend Becomes An Enemy. *Curr Protein Pept Sci.* 2017.
87. Lv X, Zhao F, Huo X, Tang W, Hu B, Gong X, et al. Neuropeptide Y1 receptor inhibits cell growth through inactivating mitogen-activated protein kinase signal pathway in human hepatocellular carcinoma. *Med Oncol.* 2016;33(7):70.
88. Park MH, Min WK, Jin HK, and Bae JS. Role of neuropeptide Y in the bone marrow hematopoietic stem cell microenvironment. *BMB Rep.* 2015;48(12):645-6.
89. Wang W, Rigueur D, and Lyons KM. TGFbeta signaling in cartilage development and maintenance. *Birth Defects Res C Embryo Today.* 2014;102(1):37-51.
90. Abou-Alfa GK, Miksad RA, Tejani MA, Williamson S, Gutierrez ME, Olowokure OO, et al. A Phase Ib, Open-Label Study of Dalantercept, an Activin Receptor-Like Kinase 1 Ligand Trap, plus Sorafenib in Advanced Hepatocellular Carcinoma. *Oncologist.* 2019;24(2):161-e70.
91. Ambrosi TH, Scialdone A, Graja A, Gohlke S, Jank AM, Bocian C, et al. Adipocyte Accumulation in the Bone Marrow during Obesity and Aging Impairs Stem Cell-Based Hematopoietic and Bone Regeneration. *Cell Stem Cell.* 2017;20(6):771-84 e6.
92. Thasler WE, Weiss TS, Schillhorn K, Stoll PT, Irrgang B, and Jauch KW. Charitable State-Controlled Foundation Human Tissue and Cell Research: Ethic and Legal Aspects in the Supply of Surgically Removed Human Tissue For Research in the Academic and Commercial Sector in Germany. *Cell Tissue Bank.* 2003;4(1):49-56.

FIGURE LEGENDS

Figure 1

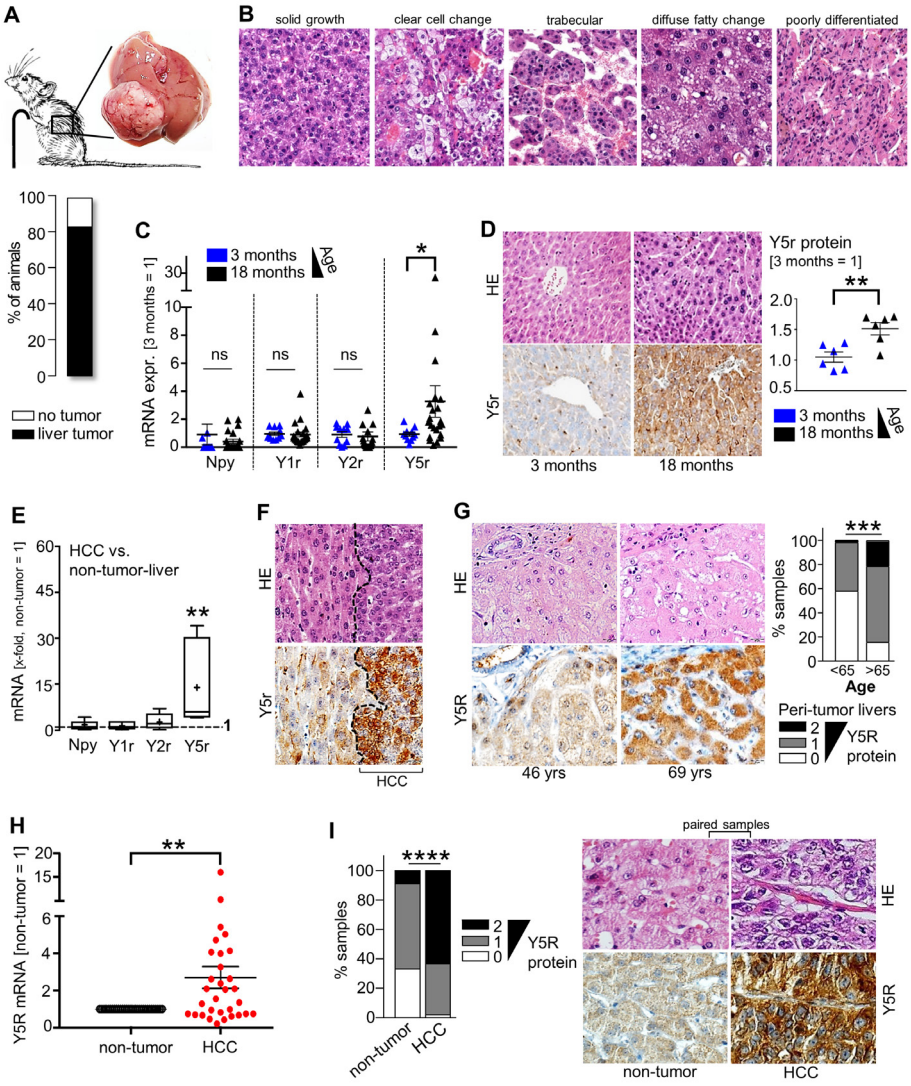

Figure 1. Upregulation of NPY5-receptor in hepatocellular carcinoma. (**A**) Explanted, tumor-bearing liver (representative image) derived from an aged C3H/HeN mouse and bar graph (below) depicting percentages of tumor-bearing mice at the age of eighteen months (*n* = 12). (**B**) Representative images (HE-staining; 20-fold magnification; *n* = 12) depicting histological heterogeneity of HCC derived from aged C3H mice. (**C**) Normalized mRNA levels of Npy, Y1r, Y2r and Y5r in non-tumorous livers comparing young (*n* = 11) with aged (*n* = 22) mice. (**D**) Representative images (10-fold magnification; HE- and Y5r-staining), and immunohistochemical analysis of Y5r protein levels in non-tumorous livers comparing young (*n* = 6) and aged (*n* = 6) mice. (**E**) Normalized Npy, Y1r, Y2r and Y5r mRNA levels in HCC compared with corresponding non-tumorous liver tissues derived from aged C3H mice (*n* = 8) (box and whisker plots (min to max), "+": mean values). (**F**) Representative images (HE- and Y5R-staining; 20-fold magnification) of age-related HCC and peri-tumorous tissues derived from C3H mice (*n* = 12). (**G**) Representative images (HE- and Y5R-staining; 40-fold magnification); Y5R protein expression (immunohistochemistry) in non-tumorous liver tissues of younger (<65 years) (*n* = 57) compared with older (>65 years) (*n* = 51) HCC patients. (**H**) Y5R mRNA levels in paired HCC and corresponding peri-tumorous ("non-tumor") liver tissues (*n* = 31 pairs). (**I**) Representative images (HE- and Y5R-staining; 40-fold magnification) and immunohistochemical analysis of Y5R protein levels in HCC compared with corresponding peri-tumorous liver tissues ("non-tumor") (*n* = 231). Data are presented as mean ± SEM. Statistical significance was determined by 2-tailed, unpaired t-test (**C**,**D**), 2-tailed, paired t-test (**E**,**H**), two-sided Fisher′s exact test together with Spearman correlation analysis (**G**,**I**) and uni- and multivariate analysis applying ordinal regression analysis (link function: logit) (**G**). **P* < 0.05, ***P* < 0.01, ****P* < 0.001, *****P* < 0.0001.

Figure 2

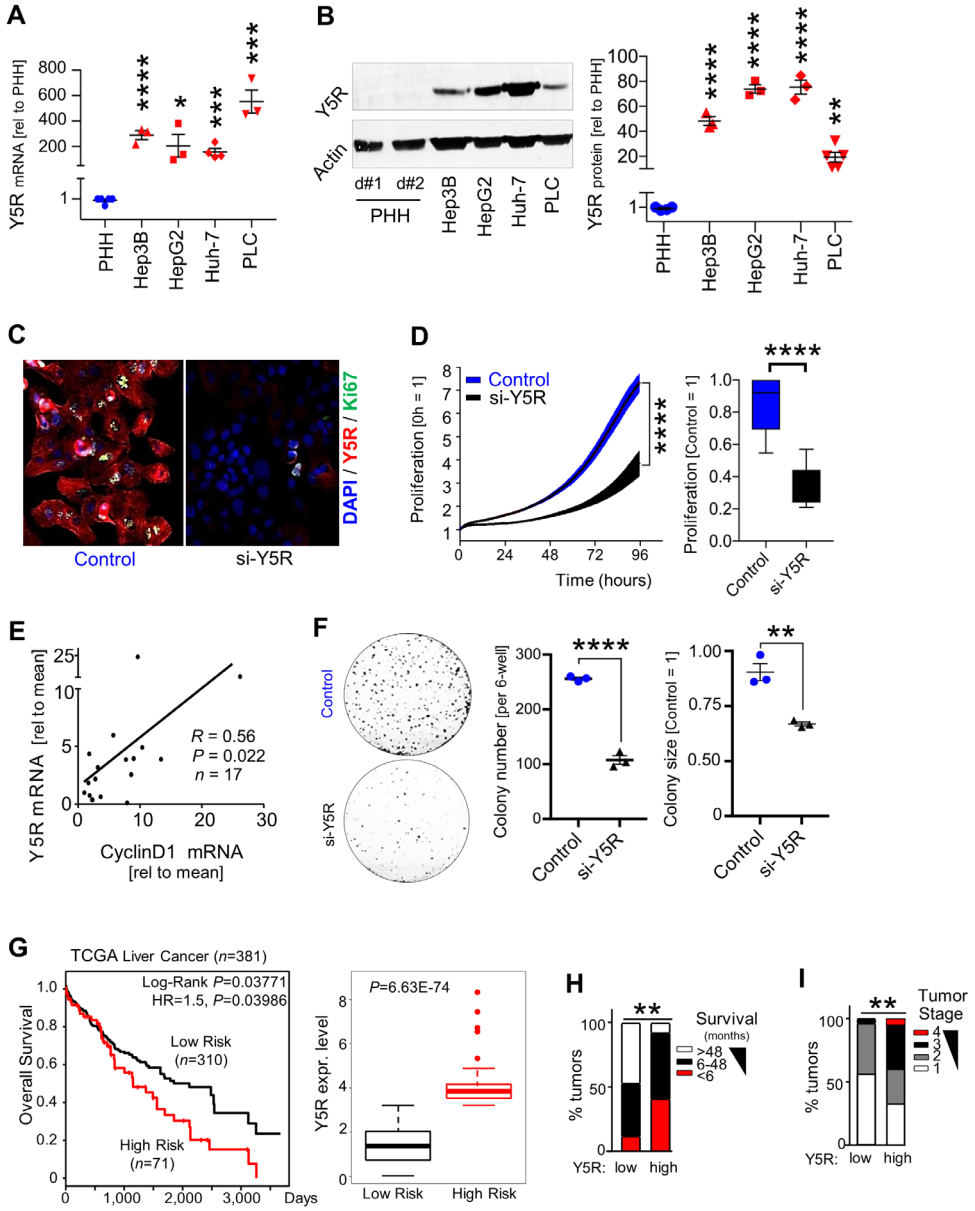

Figure 2. Y5R enhances tumorigenicity of HCC and correlates with poor survival. (**A**) Y5R mRNA levels in primary human hepatocytes (PHH) (n = 5) compared with human HCC cell lines (Hep3B (n = 3), HepG2 (n = 3), Huh-7 (n = 4), PLC (n = 3)). (**B**) Y5R Western blot analysis: representative image (PHH from two donors (d#1, d#2)) and quantification of protein levels (PHH (n = 4) compared with Hep3B (n = 3), HepG2 (n = 3), Huh-7 (n = 3), PLC (n = 5)). (**C**,**D**) HCC cells transfected with si-RNA-pools against Y5R ("si-Y5R") or a control-si-RNA-pool ("Control"). (C) Co-immunofluorescence (Y5R, Ki-67) images (20-fold magnification; n = 2). (D) Representative proliferation curves and quantification (n = 3) (box and whisker plots (min to max)). (**E**) Correlated Y5R and CyclinD1 mRNA levels in human HCC tissues (n = 17). (**F**) Clonogenicity (colony numbers, sizes, representative images) of PLC cells after RNAi-mediated Y5R-knockdown (n = 3). (**G**) "SurvExpress" database analysis of Y5R expression and overall survival (dataset from "The Cancer Genome Atlas" (TCGA); n = 381). Computational stratification ("low risk" and "high risk" groups) based on prognostic index. (**H,I**) Comparison of (H) survival of patients with low (n = 17) and high (n = 39) Y5R expression, and (I) tumor stages of patients with low (n = 25) and high (n = 92) Y5R expression based on immunohistochemical analysis of HCC tissue micro array samples. Data are presented as mean ± SEM. Statistical significance was determined by (**A**,**B**) ordinary one-way ANOVA together with Dunnett's multiple comparisons, (**D**,**F**) 2-tailed, unpaired t-test, (**E**) Pearson correlation, (**H**,**I**) two-sided Fisher's exact test, Spearman correlation and uni- and multivariate analysis applying ordinal regression analysis (link function: logit), (**G**) log-rank testing and hazard ratio estimates. *P < 0.05, **P < 0.01, ***P < 0.001, ****P < 0.0001.

Figure 3

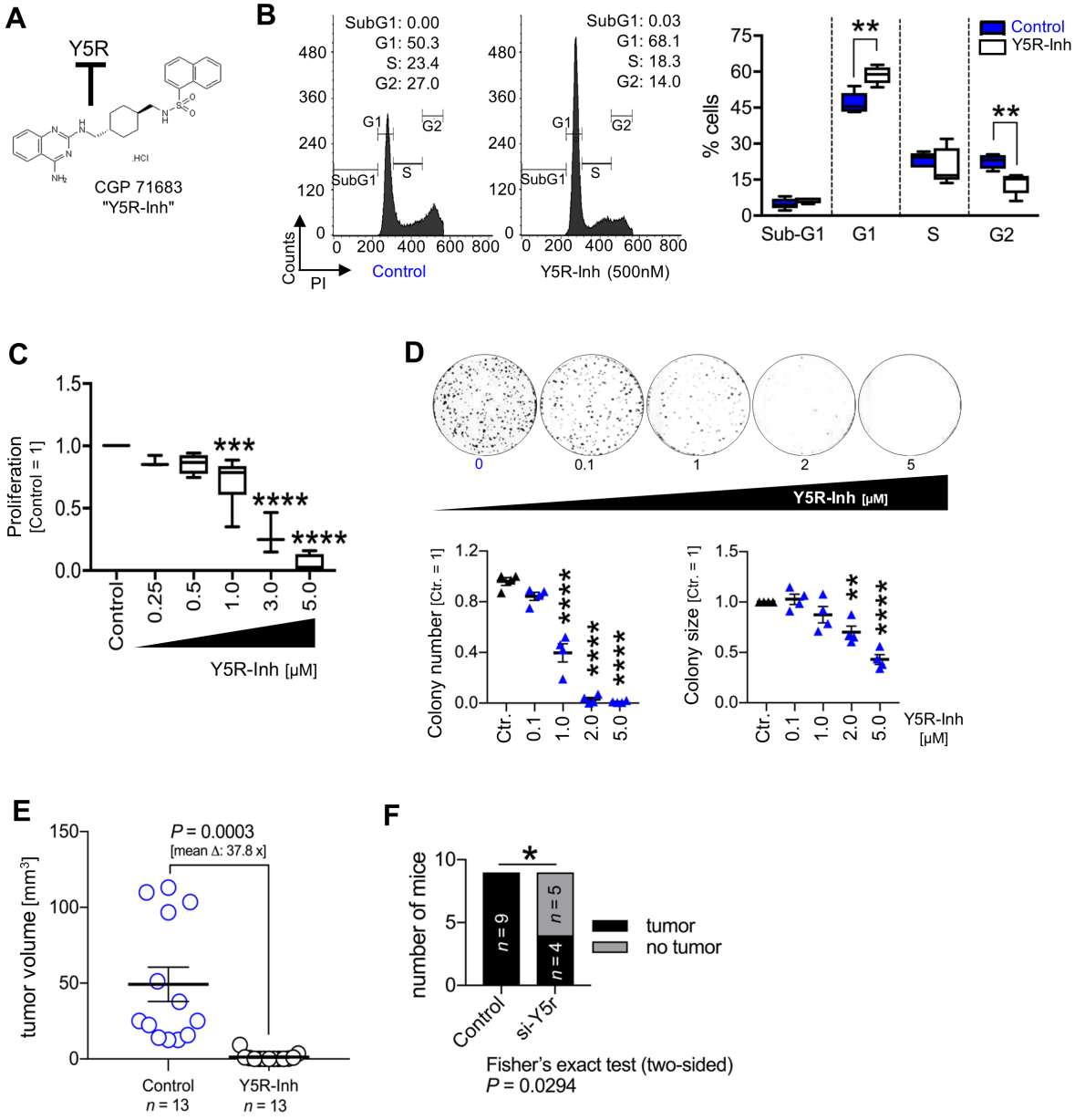

Figure 3. Y5R-inhibition impairs tumorigenicity and growth of HCC. (**A**) Chemical formula of the specific, high-affinity Y5R-inhibitor "CGP71683" (Y5R-Inh). (**B-D**) Y5R-Inh-treated as compared with control (i.e. solvent (DMSO))-treated HCC cells applying different functional in vitro assays. (B) Fluorescence-activated cell sorting (FACS) analysis (representative images and quantification) after propidium-iodide (PI) staining; quantification of SubG1/G0-, G1-, S-, and G2-cell cycle fractions (n = 3) (data are shown as box and whisker plots (min to max)). (C) Real-time proliferation analysis applying different doses of Y5R-Inh (n = 3) (data are shown as box and whisker plots (min to max)). (D) Quantification of colony numbers, sizes and representative images applying clonogenicity assays (n = 4). (**E**,**F**) Murine HCC models of orthotopic syngeneic HCC cell implantation (Hepa129 cells) in C3H mice. (E) After HCC cell implantation, mice were randomized into two groups and treated with Y5R-Inh (15 mg/kg bodyweight, daily i.p.-injection for 7 days) or received the solvent only. (F) For RNAi-mediated Y5r-knockout, transfection of HCC cells was performed for 48 hours prior to injection into livers, and tumor onset was assessed after 7 days. Data are presented as mean ± SEM. Statistical significance was determined by ordinary one-way ANOVA together with Dunnett's multiple comparisons test (**C**,**D**), 2-tailed, unpaired t-test (**B**,**E**), or by two-sided Fisher's exact test together with Spearman correlation analysis (**F**). *P < 0.05, **P < 0.01, ***P < 0.001, ****P < 0.0001.

Figure 4

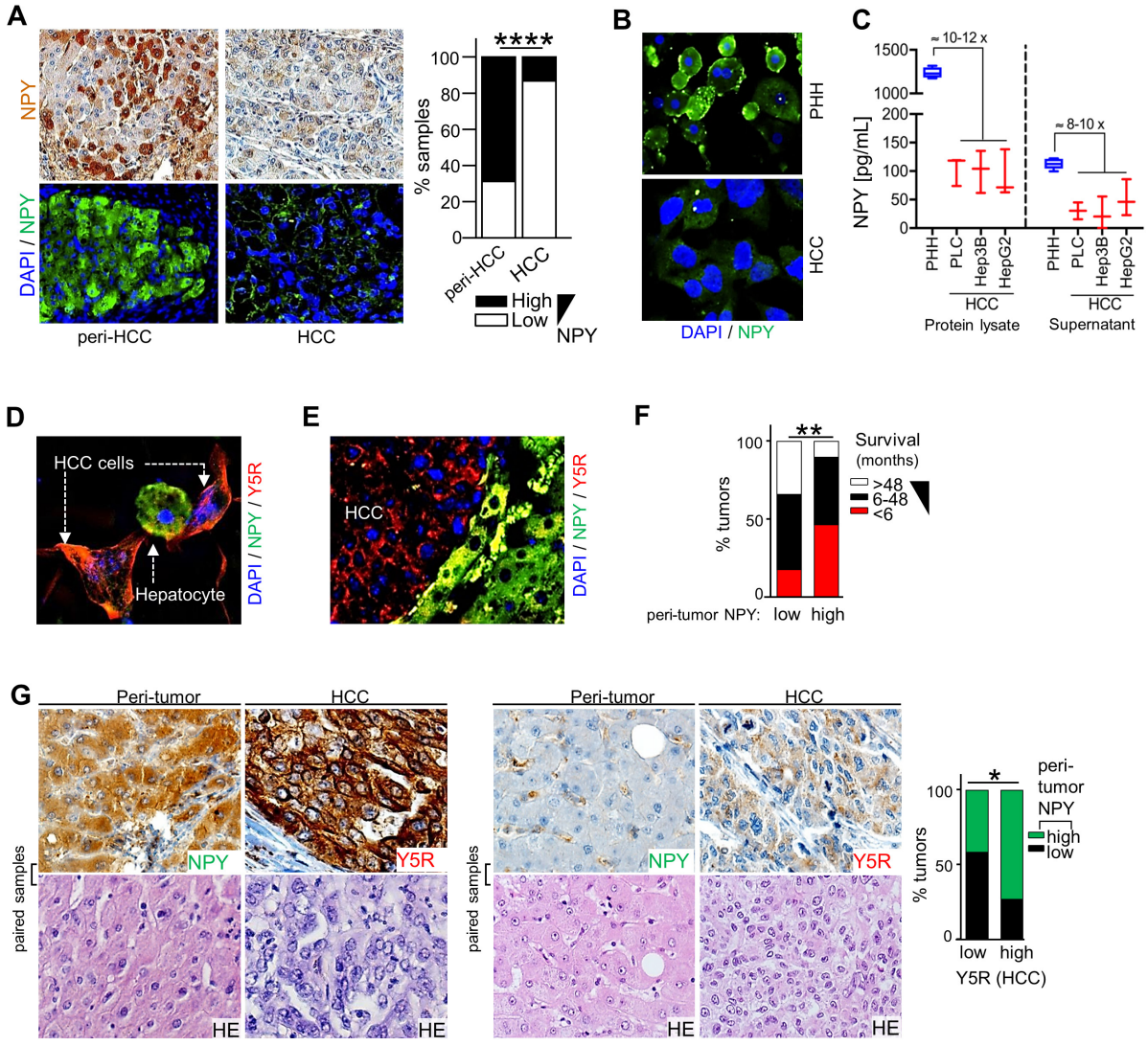

Figure 4. Neuropeptide Y is secreted by peri-tumorous hepatocytes and correlates with survival and Y5-receptor expression in HCC. (**A**,**B**) Immunohistochemical/immunofluorescence analysis of NPY expression in (A) paired non-tumorous ("peri-HCC") and HCC tissues of patients (representative images (20-fold magnification) and quantification) applying a tissue micro array (*n* = 231) and (B) representative images (40-fold magnification) displaying primary human hepatocytes (PHH) and HCC cells (Hep3B) (*n* = 3). (**C**) ELISA-analysis of NPY expression in protein lysates and in cell culture supernatants of PHH (*n* = 4) and HCC cells (PLC (*n* = 3), Hep3B (*n* = 3), HepG2 (*n* = 3)) (data are shown as box and whisker plots (min to max)). (**D**,**E**) Co-immunofluorescence staining of NPY and Y5R protein in (D) in vitro co-cultures of hepatocytes and HCC cells (*n* = 2) (40-fold magnification) and (E) the murine orthotopic HCC model (*n* = 6) (20-fold magnification). (**F**) Comparison of survival of HCC patients with high (*n* = 31) and low (*n* = 27) NPY immunoreactivity in peri-tumorous liver tissue applying a tissue micro array. (**G**) Representative images (40-fold magnification) and immunohistochemical analysis of NPY and Y5R staining of paired peri-tumorous liver tissues and corresponding HCC tissues applying a human tissue micro array (*n* = 103). Data are presented as mean ± SEM. Statistical significance was determined by two-sided Fisher's exact test together with Spearman correlation analysis (**A**,**F**,**G**) and uni- and multivariate analysis applying ordinal regression analysis (link function: logit) (**F**). **P* < 0.05, ***P* < 0.01, *****P* < 0.0001.

Figure 5

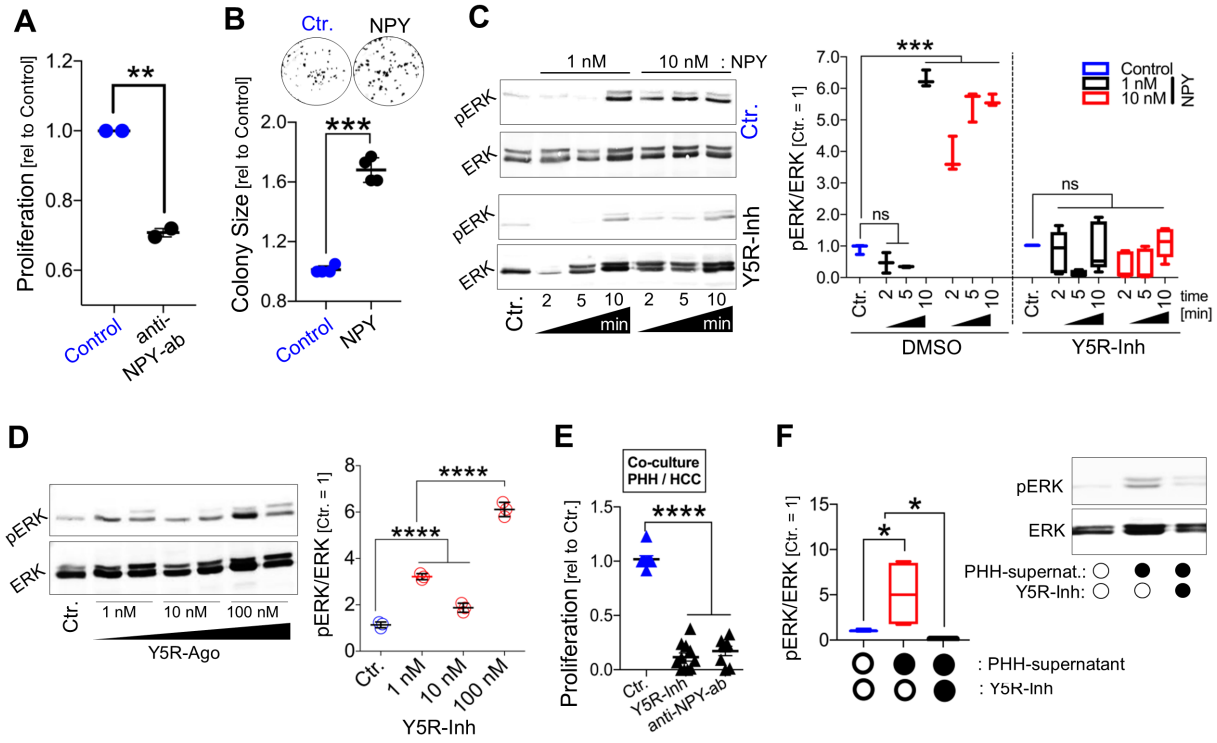

Figure 5. Neuropeptide Y cross-talks with Y5-receptor in HCC. (**A**) Real-time cell proliferation analysis of HCC cells (PLC) in serum (i.e. NPY)-containing culture medium applying an NPY-neutralizing antibody (anti-NPY-ab) (*n* = 2; two replicates per independent experiment). (**B**) Clonogenicity assay (representative images and quantification of colony sizes) of NPY-treated (500 nM) and control-treated HCC cells (PLC) applying serum-free medium (*n* = 4). (**C**,**D**) Western blot analysis of phospho-ERK (pERK) and ERK levels (representative images and densitometric quantification) of HCC cells (PLC) treated with recombinant NPY with or without combined treatment applying the specific Y5R-inhibitor "CGP71683" (Y5R-Inh) (*n* = 3) (C) (data are shown as box and whisker plots (min to max)), or treated with the specific Y5R-agonist ("BWX46") (the representative image shows duplicates for Y5R-agonist-treatment) (*n* = 3) (D). (**E**) Real-time cell proliferation analysis of co-cultured HCC cells and PHH applying the Y5R-inhibitor or a neutralizing NPY-antibody (anti-NPY-ab) as compared with control-treatment (*n* = 8). (**F**) Western blot analysis (and representative image) of pERK and ERK levels in HCC cells incubated with cell culture supernatant of PHH (containing NPY as quantified by ELISA) with or without combined treatment applying Y5R-Inh or anti-NPY-ab (*n* = 3) (data are shown as box and whisker plots (min to max)). Data are presented as mean ± SEM. Statistical significance was determined by ordinary one-way ANOVA together with Dunnett's multiple comparisons test (**C**,**D**,**F**), or by 2-tailed, unpaired t-test (**A**,**B**,**E**). **P* < 0.05, ***P* < 0.01, ****P* < 0.001, *****P* < 0.0001, ns: non-significant.

Figure 6

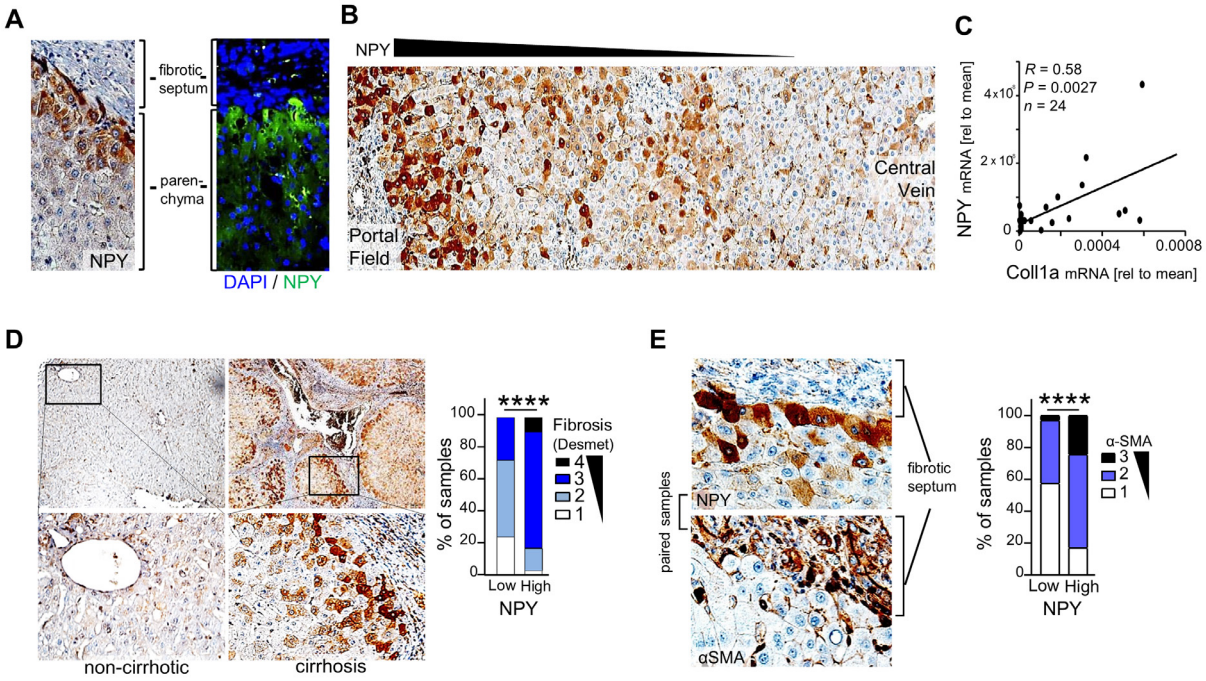

Figure 6. Peri-tumorous NPY expression by hepatocytes correlates with hepatic fibrosis. (**A**,**B**) Immunohistochemical/immunofluorescence analysis of NPY-staining (representative images, 40-fold magnification (A) and 20-fold magnification (B), respectively) of peri-tumorous liver tissues applying a tissue micro array (TMA; *n* = 231). (**C**) Paired NPY and collagen type I mRNA expression (qRT-PCR analysis) in human peri-tumorous liver tissues (*n* = 24). (**D**) Immunohistochemical analysis (representative images (10- and 40-fold magnification, respectively) and quantification) of fibrosis (applying the "Desmet" score system) in peri-tumorous liver tissues with high (*n* = 64) as compared to low (*n* = 33) NPY expression levels applying a human tissue micro array. (**E**) Immunohistochemical analysis (representative images and quantification) of α-smooth-muscle actin (αSMA) expression in peri-tumorous liver tissues with high (*n* = 58) as compared to low (*n* = 33) NPY expression levels applying a human TMA (the representative images (40-fold magnification) display the same loci derived from paired (i.e. serial) tissue sections from one patient). Data are presented as mean ± SEM. Statistical significance was determined by Pearson correlation (**C**) or by two-sided Fisher's exact test together with Spearman correlation analysis (**D**,**E**). ****$P < 0.0001$.

Figure 7

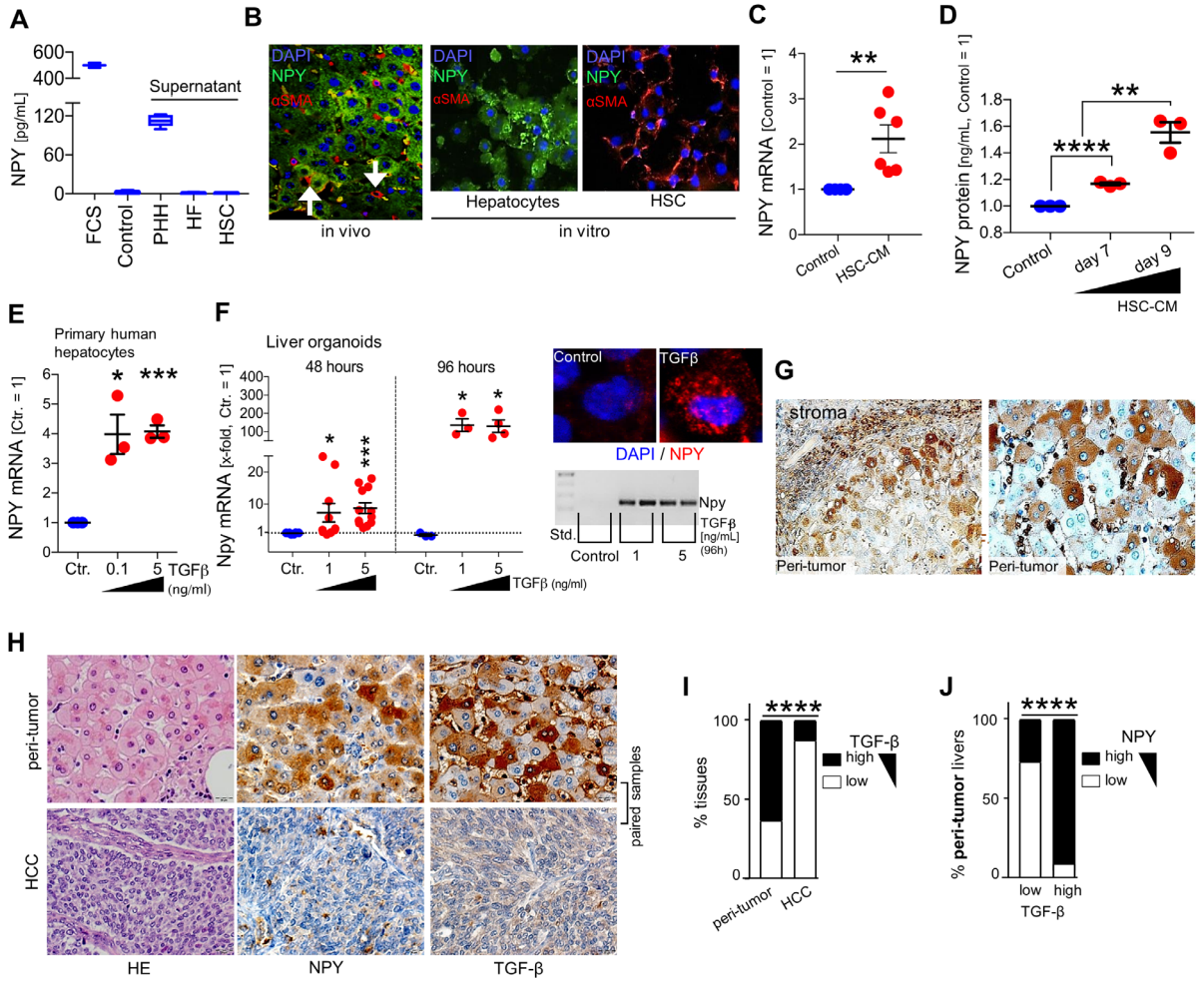

Figure 7. Peri-tumorous, hepatocyte-derived NPY expression is induced by TGFβ. (**A**) Enzyme-linked immunosorbent assay (ELISA) analysis of NPY protein levels in cell culture medium with fetal calf serum (FCS; *n* = 3), serum-free medium (Control; *n* = 3), and cell culture supernatants of primary human hepatocytes (PHH; *n* = 6), human fibroblasts (HF; *n* = 2), and hepatic stellate cells (HSC; *n* = 3). (**B**) Representative images of (co)-immunofluorescence staining (NPY and αSMA; 20-fold magnification) of peri-tumorous liver tissues of C3H mice (left, *n* = 3) and cultures PHH or HSC (*n* = 3; right). (**C**) NPY mRNA of PHH treated with or without conditioned culture medium derived from HSC (HSC-CM; *n* = 6). (**D**) NPY protein levels in cell culture supernatants treated with or without HSC-CM (*n* = 3). (**E**) NPY mRNA in PHH treated for 48 hours with different doses of TGFβ (*n* = 3). (**F**) NPY mRNA in hepatocyte-derived liver organoids treated for 48 hours (*n* = 10) or 96 hours (n = 4) with TGFβ (left). Representative images of qRT-PCR-gel-electrophoresis (*n* = 3) and confocal immunofluorescence (60-fold magnification; *n* = 2) (right). (**G**) Representative immunohistochemical TGFβ-staining of (human) peri-tumorous liver (40-fold magnification). (**H-J**) Immunohistochemical analysis of TGFβ and NPY in peri-tumorous liver and corresponding HCC tissues. (H) Representative images (40-fold magnification). (I) Comparison of TGFβ expression in HCC and corresponding peri-tumorous liver tissues (*n* = 219). (J) Comparison of NPY expression in peri-tumorous liver tissues with low (*n* = 38) and high (*n* = 63) TGFβ-expression. Data are presented as mean ± SEM. Statistical significance was determined by ordinary one-way ANOVA together with Dunnett's multiple comparisons test (**D**,**E**,**F**), 2-tailed, unpaired t-test (**C**), or by two-sided Fisher's exact test and Spearman correlation analysis (**I**,**J**). **P* < 0.05, ***P* < 0.01, ****P* < 0.001, *****P* < 0.0001.

Figure 8

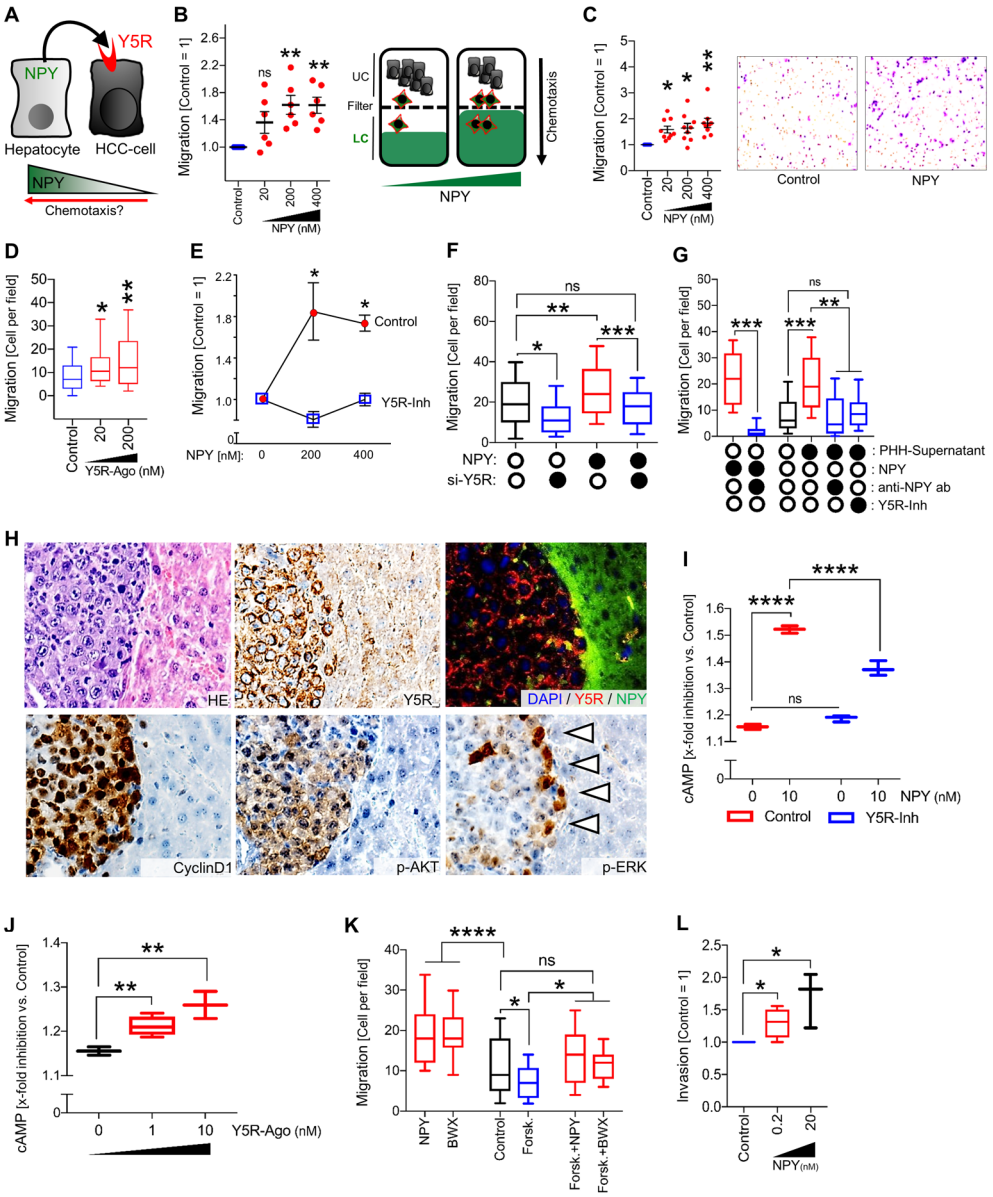

Figure 8. Hepatocyte-derived NPY mediates chemotaxis via activation of Y5R. (**A**) Cartoon illustrating the hypothesis that an NPY-gradient caused by downregulation of NPY in HCC cells and NPY expression by peri-tumorous hepatocytes impacts chemotaxis of HCC cells via Y5R-activation. (**B-G**) Real-time cell migration (B) and Boyden chamber (C-G) analysis (upper (UC) and lower (LC) chamber) of chemotaxis of HCC cells towards recombinant NPY (B (*n* = *6*), C (*n* = *8*)), (D) Y5R-agonist BWX46 (Y5R-Ago) (*n* = *3*), (E) NPY with or without Y5R-inhibition applying CGP71683 (Y5R-Inh) (*n* = *3*), (F) NPY and/or si-RNA-pool-mediated Y5R-knockdown (*n* = *3;* box and whisker plots (min to max)). (G) NPY or supernatants of primary human hepatocytes (PHH) with or without Y5R-Inh or an NPY-neutralizing antibody (anti-NPY-ab); (*n* = 3, box and whisker plots (min to max)). (**H**) Representative immunohistochemical (HE, Y5R, CyclinD1, pAKT, pERK) and co-immunofluorescence (Y5R and NPY) analysis (serial sections) of HCC and peri-tumorous liver tissue in the orthotopic murine HCC model (20-fold magnification; *n* = 6). Arrowheads depict the tumor-parenchyma edge. (**I**,**J**) cAMP-signaling (analyzed by Bioluminescence resonance energy transfer technique) of PLC cells (I) treated with NPY and/or Y5R-Inh or (J) different doses of Y5R-Ago (box and whisker plots (min to max); *n* = 3). (**K**) Boyden chamber analysis of migration of HCC cells towards NPY or BWX46 with or without co-treatment with the cAMP-inductor forskolin (Forsk.) (*n* = 4, box and whisker plots (min to max)). (**L**) Boyden chamber analysis of invasion of HCC cells towards NPY in the lower compartment (*n* = 4, box and whisker plots (min to max)). Data are presented as mean ± SEM. Statistical significance was determined by ordinary one-way ANOVA together with Dunnett's multiple comparisons test (**B**,**C**,**D**,**E**,**F**,**G**,**I**,**J**,**K**,**L**). **P* < 0.05, ***P* < 0.01, ****P* < 0.001, *****P* < 0.0001, ns: non-significant.

Figure 9

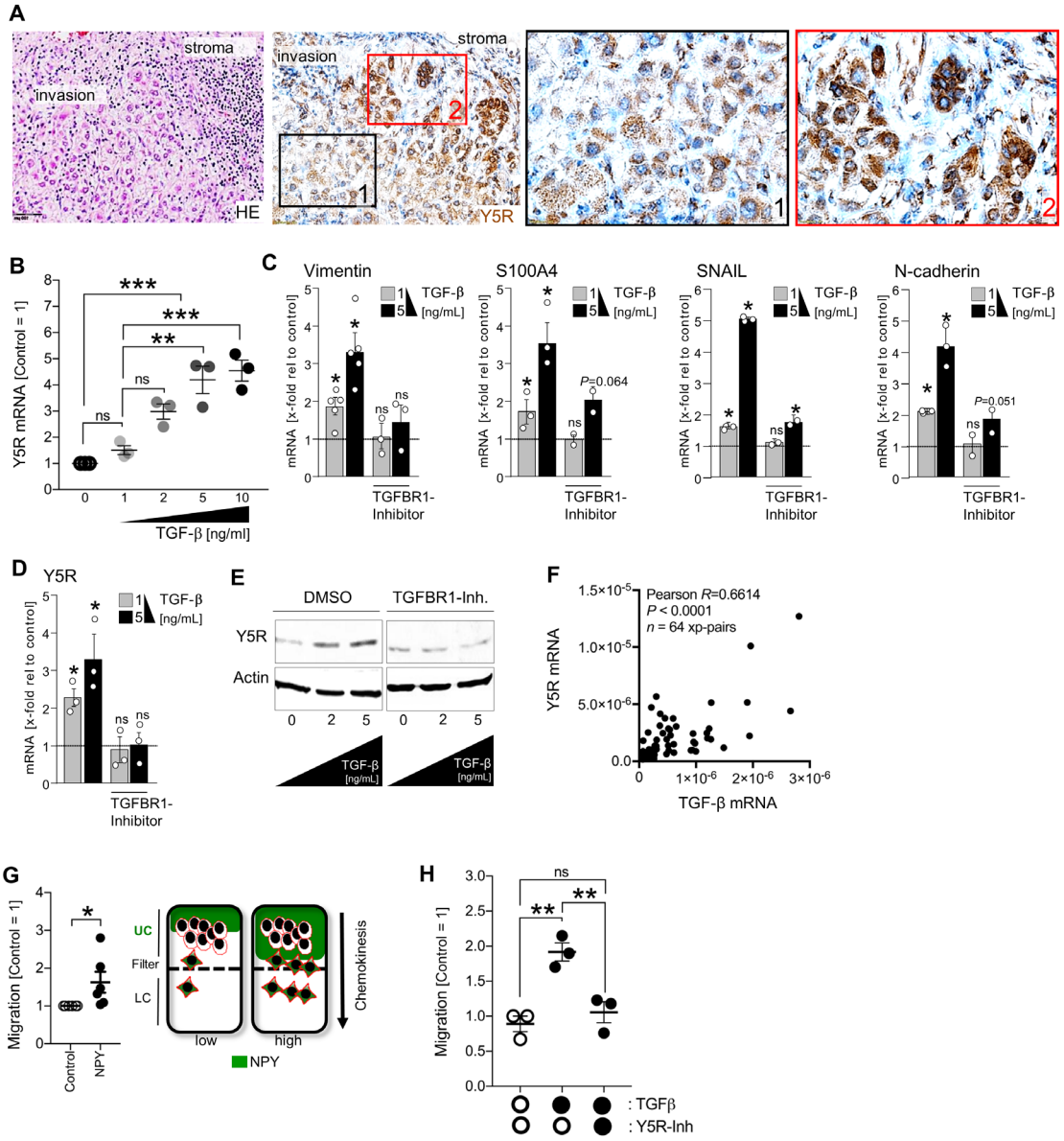

Figure 9. Y5R expression in HCC cells at sites of stroma-invasion and TGFβ-mediated effects on Y5R expression in HCC cells. (**A**) Representative images of Y5R (and HE)-immunostaining (10- and 40-fold magnification, respectively) of human HCC tissues at sites of stroma-infiltration (n = 122). (**B**) Y5R mRNA expression (qRT-PCR analysis) levels in HCC cells (PLC) treated with different doses of recombinant TGFβ (n = 3). (**C,D**) mRNA expression levels (qRT-PCR analysis) of (C) epithelial-mesenchymal-transition (EMT)-markers (Vimentin, S100A4, SNAIL and N-cadherin) and (D) Y5R in HCC cells (PLC) after 96 hours of treatment with recombinant TGFβ with or without co-treatment with the specific TGFβ-receptor 1 (TGFBR1)-inhibitor galunisertib (10 µM) (n = 3). (**E**) Western blot analysis (representative images, n = 3) of Y5R protein levels in HCC cells after treatment with different doses of TGFβ (96 hours), with or without co-treatment with galunisertib (10 µM). (**F**) Paired Y5R and TGFβ mRNA expression analysis (qRT-PCR analysis, relative to β-Actin) in HCC patient tissues (n = 64). (**G**) Real-time cell migration (xCELLigence) analysis of HCC cells (PLC) which were treated with low-dose recombinant NPY (10 nM) to induce non-directed migration (i.e. "chemokinesis") (n = 6). (**H**) Boyden chamber analysis of chemokinesis of HCC cells (PLC) treated with or without recombinant TGFβ (5 ng/ml) and/or the specific Y5R-inhibitor "CGP71683" (Y5R-Inh). (n = 3). Data are presented as mean ± SEM. Statistical significance was determined by ordinary one-way ANOVA together with Dunnett's multiple comparisons test (**B**,**C**,**D**,**H**), 2-tailed, unpaired t-test (**G**), or Pearson correlation (**F**). *P < 0.05, **P < 0.01, ***P < 0.001, ns: non-significant.

Figure 10

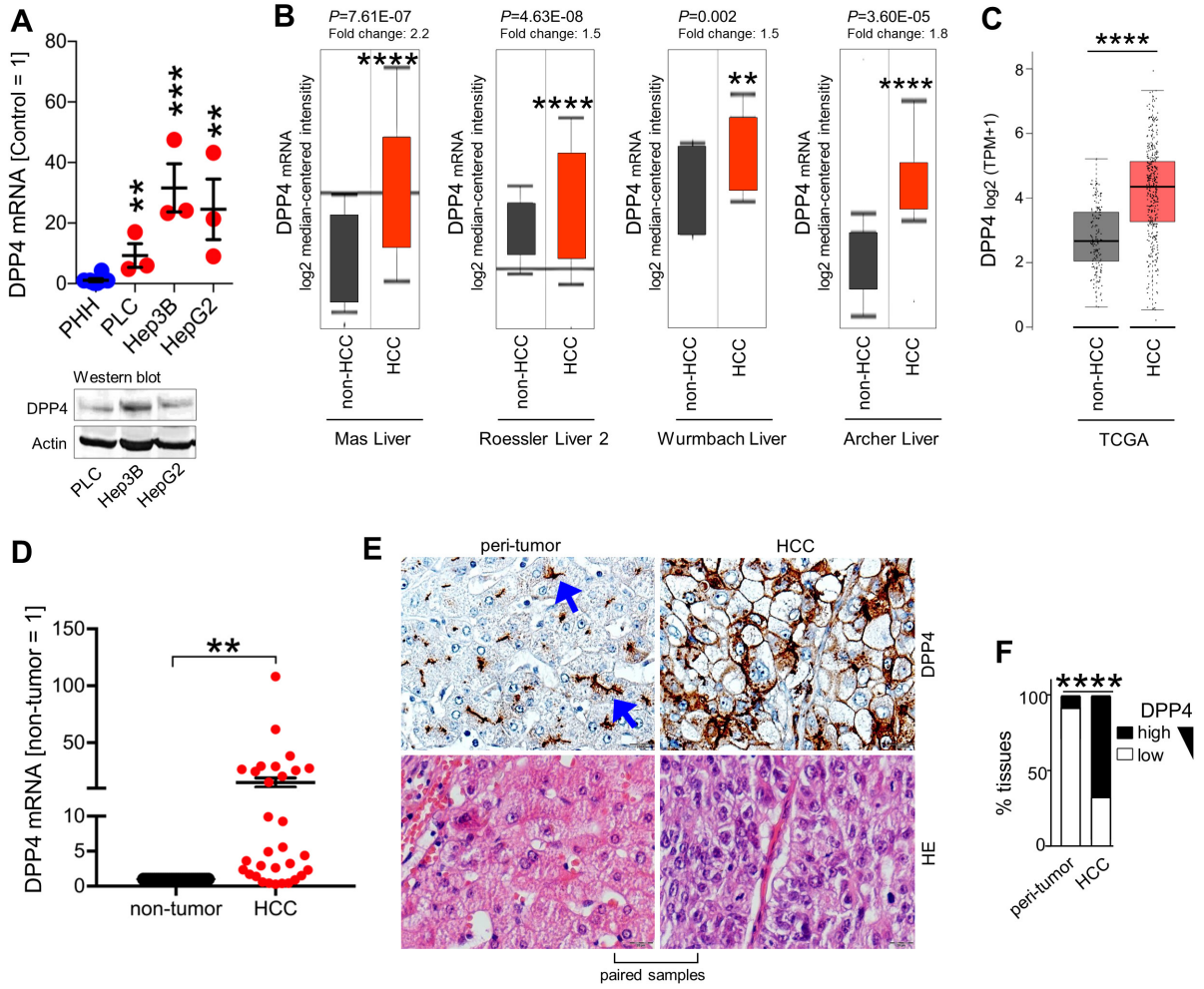

Figure 10. Dipeptidylpeptidase 4 (DPP4) is overexpressed in hepatocellular carcinoma. (**A**) DPP4 mRNA expression (qRT-PCR) in human HCC cell lines (PLC (*n* = 3), Hep3B (*n* = 3), HepG2 (*n* = 3)) compared with primary human hepatocytes (PHH, *n* = 5); below, representative Western blot images depicting DPP4 protein expression in HCC cells (*n* = 2). (**B**) DPP4 RNA expression levels in HCC compared with non-tumorous liver tissues (non-HCC) in different patient datasets ("Mas Liver", non-HCC: n = 19, HCC: n = 38; "Roessler Liver 2", non-HCC: n = 220, HCC: n = 225; "Wurmbach Liver", non-HCC: n = 10, HCC: n = 35; "Archer Liver", non-HCC: n = 47, HCC: n = 16) applying the Oncomine™ database (box and whisker plots (min to max)). (**C**) Y5R expression in TCGA-derived HCC tissues (*n* = 369) compared with matched non-tumorous liver tissues (non-HCC) (*n* = 160) applying the "Gene Expression Profiling Interactive Analysis" (GEPIA) database. The expression data were first log_2(TPM+1) transformed for differential analysis. (**D**) DPP4 mRNA expression (quantified by quantitative RT-PCR analysis) in paired human HCC and corresponding peri-tumorous liver tissues ("non-tumor") (*n* = 31). (**E**) Representative immunohistochemical DPP4 staining (and HE-staining) (40-fold magnification) in HCC and corresponding peri-tumorous liver tissues of the same patients (*n* = 213). Blue arrows depict the typical bile-canalicular staining pattern of DPP4 in non-tumorous hepatocytes. (**F**) Quantification of immunohistochemical DPP4 expression in HCC compared to corresponding peri-tumorous liver tissues of the same patients (*n* = 213). Data are presented as mean ± SEM. Statistical significance was determined by ordinary one-way ANOVA together with Dunnett's multiple comparisons test (**A**,**C**), 2-tailed, unpaired t-test (**B**), 2-tailed, paired t-test (**D**), or by two-sided Fisher's exact test together with Spearman correlation analysis (**F**). ***P* < 0.01, ****P* < 0.001, *****P* < 0.0001.

Figure 11

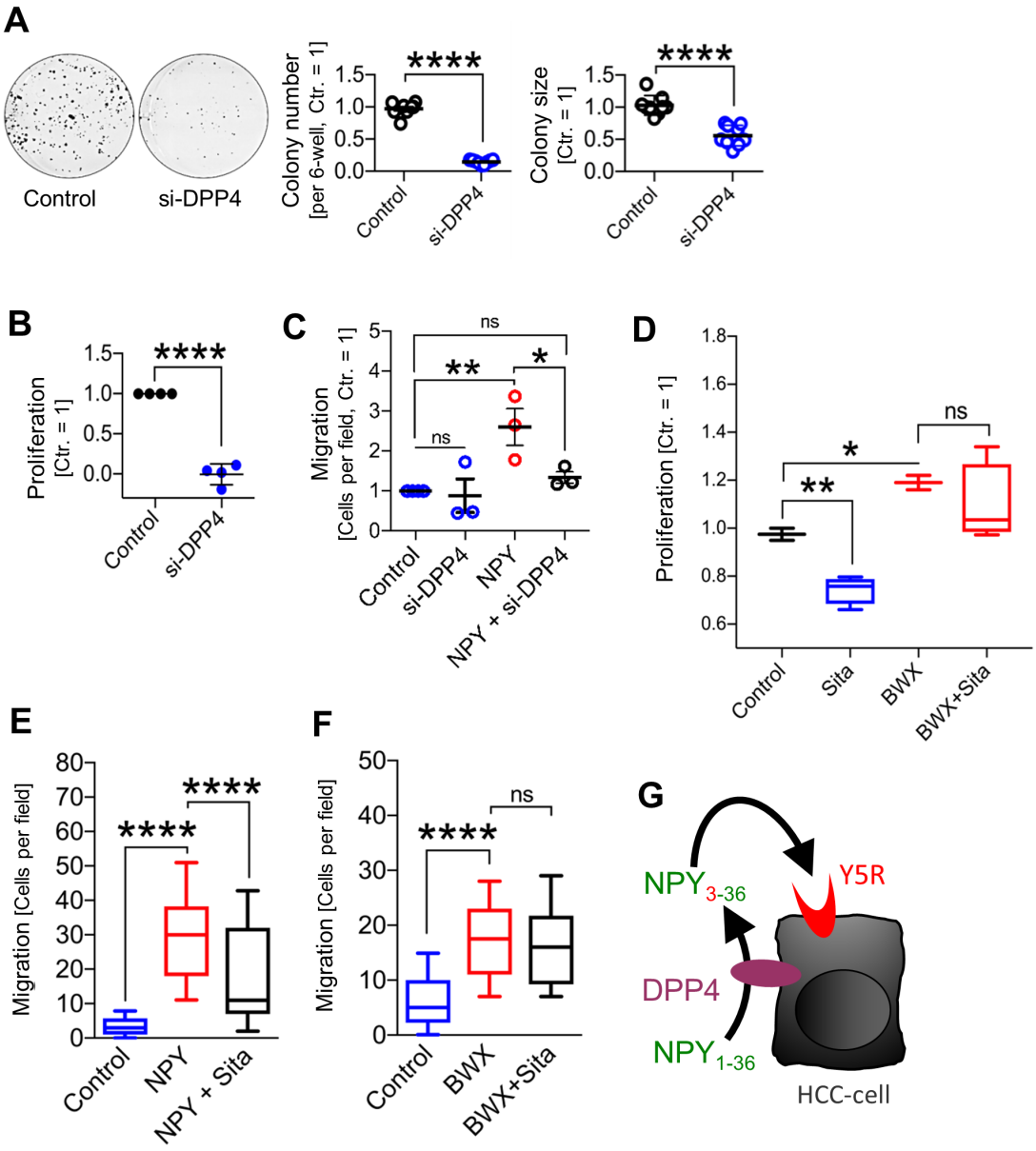

Figure 11. Y5R-activation is augmented by dipeptidylpeptidase 4 in HCC. (**A**-**C**) HCC cells were transfected with si-RNAs against human DPP4 ("si-DPP4") or with control-si-RNAs ("Control"). (A) Clonogenicity assays (quantified colony numbers and sizes (right panels) and representative images (left panels, e.g. Hep3B) of HCC cells (summarized data for Hep3B (*n* = 6) and PLC (*n* = 3)). (B) Real-time cell proliferation analysis (PLC (*n* = 4)). (C) Boyden chamber analysis of chemotactic (i.e. directed) migration of HCC cells (PLC) towards control-medium or a gradient induced by recombinant NPY (100 nM) with or without combined RNAi-mediated DPP4-knockdown (*n* = 3). (**D**) Real-time proliferation analysis (xCELLigence) of HCC cells (PLC) using serum-containing (i.e. NPY-containing) culture medium and treatment with sitagliptin (1 µM) with or without co-treatment with the specific Y5R-agonist BWX46 (200 nM) (*n* = 4; box and whisker plots (min to max)). (**E**,**F**) Boyden chamber analysis of HCC cells (PLC) migrating towards a gradient induced by (E) recombinant NPY (100 nM) or (F) BWX46 (200 nM) with or without co-treatment with sitagliptin (1 µM) (*n* = 4; box and whisker plots (min to max)). (G) Summary and cartoon depicting the hypothesis that DPP4-mediated NPY-conversion to (more Y5R-specific) truncated NPY_{3-36} results in augmented Y5R-activation. Data are presented as mean ± SEM. Statistical significance was determined by ordinary one-way ANOVA together with Dunnett's multiple comparisons test (**C**,**D**,**E**,**F**), 2-tailed, unpaired t-test (**A**,**B**). **P* < 0.05, ***P* < 0.01, *****P* < 0.0001, ns: non-significant.

GRAPHICAL ABSTRACT